Magnetic field spectral crossings of Luttinger holes in quantum wells

G. E. Simion and Y. B. Lyanda-Geller*

Department of Physics and Astronomy and Birck Nanotechnology Center, Purdue University, West Lafayette, Indiana 47907 USA

(Received 30 June 2014; published 7 November 2014)

We develop an analytic approach to two-dimensional (2D) holes in a magnetic field that allows us to gain insight into physics of measuring the parameters of holes, such as cyclotron resonance, Shubnikov-de Haas effect and spin resonance. We derive hole energies, cyclotron masses, and the g factors in the semiclassical regime analytically, as well as analyze numerical results outside the semiclassical range of parameters, qualitatively explaining the experimentally observed magnetic field dependence of the cyclotron mass. In the semiclassical regime with large Landau level indices, and for size quantization energy much bigger than the cyclotron energy, the cyclotron mass coincides with the in-plane effective mass, calculated in the absence of a magnetic field. The hole g factor in a magnetic field perpendicular to the 2D plane is defined not only by the constant of direct coupling of the angular momentum of the holes to the magnetic field, but also by the Luttinger constants defining the effective masses of holes. We find that the g factor for quasi-2D holes with heavy mass in the [001] growth direction in GaAs quantum well is $g = 4.05$ in the semiclasssical regime. Outside the semiclassical range of parameters, holes behave as a species completely different from electrons. Spectra for size- and magnetic-field-quantized holes are nonequidistant, not fanlike, and exhibit multiple crossings, including crossing in the ground level. We calculate the effect of Dresselhaus terms, which transform some of the crossings into anticrossings, and the effects of the anisotropy of the Luttinger Hamiltonian on the 2D hole spectra. Dresselhaus terms of different symmetries are taken into account, and a regularization procedure is developed for the k_z^3 Dresselhaus terms. Control of the nonequidistant levels and crossing structure by the magnetic field can be used to control the Landau level mixing in hole systems, and thereby control hole-hole interactions in the magnetic field.

DOI: 10.1103/PhysRevB.90.195410 PACS number(s): 71.70.Ej, 76.40.+b, 76.30.−v, 78.67.−n

I. INTRODUCTION

In recent years, investigation of physical phenomena associated with symmetry and topology lead to remarkable developments in condensed matter and atomic physics, and several of these phenomena are due to the exquisite properties of spin-orbit interactions. Among the most interesting effects are realizations of Majorana fermions in solid state and atomic systems [1,2], realization of spin-orbit Bose-Einstein condensates [3], transport in topological insulators [4,5], long spin coherence in quantum bit systems [6,7], and spin-orbit interference effects [8]. One of the intriguing systems with extraordinarily strong spin-orbit interactions is valence band charge carriers (holes) in III-V, II-VI, and silicon and germanium structures, where many of these topological, coherence, and interference phenomena can manifest themselves.

The valence-band spectrum, with its remarkable spin-3/2 heavy and light branch structure, are known to lead to many spectacular phenomena in semiconductor physics since the 1950's, when understanding the hole spectrum had been a triumph of theory of symmetry of crystals. Low-dimensional holes have been investigated since the 1970's, and many signature phenomena, such as the quantum Hall effect [9], Shubnikov-de Haas oscillations [10,11], magnetic focusing [12], metal-insulator transition [13], weak localization and antilocalization in electric transport [14,15], and various resonance and optical phenomena [16] have been studied. Despite considerable effort, detailed understanding of hole systems remains a challenge. Many questions that for the world of conduction electrons in two dimensions (2D) have been long resolved, such as effective masses of charge carriers and their spin splitting in a magnetic field, still pose problems and remain controversial when it comes to 2D charge carrier holes.

Having in mind the long-term goal of finding new topological and correlated phenomena in charge carrier hole and related systems, it is important to understand in what conditions we can think of holes as reminiscent of electrons, and when holes behave as a completely different species. Although a certain understanding that holes are different exists already, we will show here that the reality is much more dramatic than realized to date. Specifically, we will investigate the spectrum of 2D hole systems in perpendicular magnetic fields, and, besides numerical study, will develop a fully analytic approach to 2D holes in a magnetic field that will allow us to gain insight into the physics of measuring the parameters of holes, such as cyclotron resonance, Shubnikov-de Haas effect and spin transport spectroscopy or spin resonance.

Understanding spectroscopic experiments in two-dimensional hole structures, and the parameters extracted from those experiments, is important for the following reasons. First, the two-dimensional systems themselves can potentially be used for making experimental settings, in which new topological objects such as, e.g., Majorana fermions would manifest themselves. Properties of some of these settings may directly be related to values of effective two-dimensional g factors, masses, and effective spin-orbit constants. A problem arises: which values of the parameters of 2D hole gas, and which regimes of experiments that measure these parameters should be the basis of modeling these new topological objects. Second, two-dimensional systems serve as a starting point for many theoretical considerations of 1D and 0D objects, quantum dots and wires, which in turn can be used to design systems with quantum bits and various spintronic devices.

*yuli@purdue.edu

The problem is, what are the parameters that should be used in those models, and how are they related to parameters obtained from spectroscopic measurements in 2D structures. We will see that simplified models of 2D hole systems [17–26] have to be adjusted in order to capture the true nature of holes. Third, our understanding of particle interactions, and the possibilities to control these interactions is often based on an understanding of single-particle properties. It is therefore of utmost importance to be able to extract ingredients for models of interactions from spectroscopic experiments.

The most important spectroscopic data are the energy level splitting, the resulting cyclotron mass, the resulting g factor characterizing spin splitting, and additional, e.g., spin-orbit, spectral constants. Several researchers have used numerical simulations of 3D holes to obtain quasi-2D hole spectra, see, e.g., Refs. [27–31]. However, the results of these simulations, although quite illuminating, often fail to explain experimental data even qualitatively [31]. An example of the most obvious and important question that arises is how the cyclotron mass is related to the effective 2D "band" mass? Our analytical consideration presented in this paper points to the solution of this and similar questions. We will show that the cyclotron mass in the semiclassical regime is exactly the in-plane band mass. We will also demonstrate why in most cases the cyclotron mass is continuous and does not change when the integer part of the number of filled hole levels changes in magnetic field. Furthermore, our numerical approach allows us to shed light on what spin levels are coupled by ac magnetic field in various regimes. We will derive an analytical expression, besides numerical calculation, for the g factor of holes. Contrary to a wide-spread belief [32], the g factor of 2D holes in a magnetic field in the growth direction is not defined exclusively by a constant that couples the angular momentum of the hole to the magnetic field, but also depends on constants describing the orbital motion.

How does one approach the problem of holes in two dimensions? The celebrated Γ_8 valence band Luttinger Hamiltonian [33] near the center of the Brillouine zone Γ in bulk crystals is given by

$$\mathcal{H}_L = \frac{\hbar^2}{2m_0}\left[\left(\gamma_1+\frac{5}{2}\gamma_2\right)\hat{\mathbf{k}}^2 I - 2\gamma_2\sum_i \hat{k}_i^2 J_i^2 - 4\gamma_3\sum_{i>j}\hat{k}_i\hat{k}_j J_i J_j\right], \quad (1)$$

where $\mathbf{k}$ is the wave vector, m_0 is the free electron mass, γ_1, γ_2, and γ_3 are Luttinger constants describing the hole spectrum, $i,j = x,y,z$ are principal axes of the underlying semiconductor system with $x||[100]$, J_i are the $3/2$ angular momentum matrices, and I is the identity matrix. We will consider quantum wells in semiconductor structures quantized in the z direction, i.e., grown along crystalographic direction [001].

Why is there a significant difference between 2D electrons and holes? While for bulk charge carriers the answer is transparent, simplified models in the 2D case treat 2D holes almost identically to 2D electrons. For conduction electrons with the Hamiltonian $H_e = \frac{\hbar^2}{2m_e}\hat{\mathbf{k}}^2$, where m_e is the effective electron mass, the transition to the effective electron Hamiltonian in two dimensions follows simple steps. First, one finds the wave functions of the size quantized levels in the direction of quantization, e.g., $\psi(z) = \sqrt{2/\pi}\cos\pi z/L$ for the ground level in an infinite rectangular quantum well of width L with boundaries $-L/2$ and $L/2$, and then projects the Hamiltonian integrating over z direction. If the electron Hamiltonian contains, e.g., the Dresselhaus term $H_{so} = \hbar/2\sum_i \sigma_{\mathbf{i}} p_i(p_{i+1}^2 - p_{i+2}^2)$, then the common procedure for obtaining the effective 2D electron Hamiltonian is to discard the terms linear in k_z, because $\langle k_z\rangle = 0$, where $\langle\rangle$ denotes integrating over z, and retain terms independent of z and quadratic in k_z, using the identity $\langle k_z^2\rangle = (\pi/L)^2$ for the ground quantization level. Numerous studies of the past decade or so follow the same prescription in order to obtain the 2D effective hole Hamiltonian from the bulk Hamiltonian (1), dropping terms containing $\langle k_z\rangle$ and keeping terms independent of k_z and terms with k_z^2. The simple resulting picture in the leading approximation is the ground-state hole Hamiltonian $H = \frac{\hbar^2}{2m_W}\hat{\mathbf{k}}^2$, where $m_W = m_0/(\gamma_1+\gamma_2)$ is the 2D hole mass in such an approach [32]. That is, 2D holes are treated very similarly to 2D electrons. However, this approach, valid for electrons, turns out to be incorrect in the case of holes. The crucial feature of the hole Hamiltonian (1) are terms linear in k_z and linear in the in-plane momentum. As we now illustrate, these terms contribute critically to the effective mass. Their inclusion is also crucial to the evaluation of the other parameters of 2D holes. Furthermore, what makes the situation nontrivial is that calculating the hole parameters within the framework of perturbation theory, it is necessary to take into account an infinite number of contributing terms. Indeed, the off-diagonal operators, e.g., $\{J_x J_z\}k_x k_z$ have nonzero matrix elements between simplified basis functions describing different levels of size quantization, $\psi_{h1} = \cos\pi x/L(1,0,0,0)$ and $\psi_{l2} = \cos 2\pi x/L(0,1,0,0)$, with $\langle h1|\{J_x J_z\}k_x k_z|l2\rangle \propto k_x/L$, where $|h1\rangle$ is the ground state in the z direction with heavy mass and $|l2\rangle$ is the first excited state for holes in the z direction with light mass. The second order perturbation correction to energy $\delta E = |\langle h1|\{J_x J_z\}k_x k_z|l2\rangle|^2/(E_{h1} - E_{l2})$ is proportional to the in-plane k^2 and does not contain L, because the energy separation is $E_{h1} - E_{l2} \propto (1/L^2)$. Therefore such a second-order contribution to the effective mass is as important as the first-order m_W itself. Moreover, such an off-diagonal operator has nonzero matrix elements between the $h1$ state and $|l4\rangle, |l6\rangle, \ldots, |l(\text{even})\rangle$ states, such that all second order "corrections" have the same order of magnitude, and finding the effective mass requires the summation of an infinite number of terms, which are parametrically the same.

To obtain correct results for the parameters of 2D holes in the Luttinger model (1), instead of the simplified approach, we advance a nonperturbative solution to the problem. Energies of 2D holes in a nonperturbative approach were in fact found as early as 1970 by Nedoresov [34]. The essence of such a nonperturbative approach for holes is taking into account of the mutual transformation of heavy and light holes upon reflection from the walls of the quantum well [35,36], see Fig. 1. Explicit expressions for the wave functions in the absence of the magnetic field were found in Ref. [35] where interband optical transitions were studied. In the wave functions, instead of a single standing wave in quantization direction, as is the case for electrons and simplified treatment of holes, two standing waves, one for z-direction heavy holes and one for

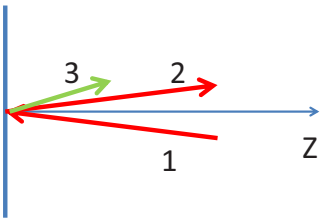

FIG. 1. (Color online) Schematic representation of the transformation of heavy holes (1) into heavy holes (2) and light holes (3) upon reflection from the quantum well interface.

z-direction light holes generally characterize every component of the wave-function spinors. Recently, one of the authors of the present article used the nonperturbative approach for calculating hole spin decoherence times in quantum dots at zero magnetic field [37].

The nonperturbative approach is central to our present study of 2D holes in a perpendicular magnetic field. We will see that the magnetic field spectra and wave functions of the holes reveal new features arising from mutual transformations of heavy and light carriers and strong spin-orbit effects. The key difference of holes from electrons is as follows: while electrons are characterized by a Landau "fan" of levels, each level being spin split due to the Zeeman effect, arising from the in-plane Hamiltonian in a magnetic field $H_e^B = \hbar^2(\mathbf{k} - e\mathbf{A}/\hbar c)^2/2m_e + g\mu\sigma\cdot\mathbf{B}$, the spectra of holes in a magnetic field generally cannot be described by a procedure that starts with the in-plane Hamiltonian and a full three-dimensional treatment is required. We shall see that for low-lying levels, there is no Landau fan for Luttinger holes and there are multiple crossings of levels as seen in Fig. 2, left panel. In the right panel, we show the traditional electron Landau fan spectrum with a small spin splitting of Landau levels characteristic of electrons in GaAs. Our analytical approach will demonstrate that only in a very narrow region of parameters, for high Landau indices and hole in-plane energies much smaller then the energy of size quantization of the holes, do holes resemble electrons. Their semiclassical spectra are obtained via a similar procedure to that for electrons, but the cyclotron and effective mass and the g factor are strongly influenced by mutual transformation of heavy and light holes in reflection from the quantum well walls.

Our ultimate goal is to consider the hole-hole interactions, but in order to put a reasonable limit to the size of this paper, we will devote a separate paper to interaction effects. Both the Hartree and exchange terms are important in a treatment of the hole-hole interactions, and we will treat them on equal footing. The scope of the present paper is restricted to the single-particle spin-orbit phenomena. The electron-phonon interactions, which are known to modify the quasiparticle spectra near the crossing of Landau levels belonging to a different size-quantization subbands, and used to probe many-body gaps in electron magnetic spectra [38,39], are also beyond the scope of the present work.

The paper is organized as follows. The Luttinger Hamiltonian and its general solution in a magnetic field perpendicular to the plane of the 2D hole gas are introduced in Sec. II, the semiclassical approximation is described in Sec. III, semiclassical spectra and numerically calculated spectra are presented in Sec. IV. Particular attention is paid to the effective mass in Sec. V, and to the Landè factor in Sec. VI. We analyze the effects of Dresselhaus interactions, arising from the absence of a center of spatial inversion in bulk materials and the effects of anisotropy of 2D hole spectra in Sec. VII. In Sec. VIII, we simulate the pattern of Shubnikov-de Haas oscillations. Evaluation of certain integrals, questions of boundary conditions and regularization of the k_z^3 Dresselhaus spin-orbit interactions are relegated to the appendices.

II. HAMILTONIAN AND WAVE FUNCTIONS FOR QUASI-TWO-DIMENSIONAL HOLES

The single-particle problem of valence band electrons in a III-V, II-VI, or Si-Ge system semiconductor in the presence of magnetic field is described by the Hamiltonian [33]

$$\hat{H}_0 = \frac{\hbar^2}{2m_0}\Big[\Big(\gamma_1 + \frac{5}{2}\gamma_2\Big)\hat{\mathbf{k}}^2 I - 2\gamma_2\big(\hat{k}_x^2 J_x^2 + \hat{k}_y^2 J_y^2 + \hat{k}_z^2 J_z^2\big) - 4\gamma_3(\{\hat{k}_x,\hat{k}_y\}\{J_x,J_y\} + \{\hat{k}_y,\hat{k}_z\}\{J_y,J_z\} + \{\hat{k}_z,\hat{k}_x\}\{J_z,J_x\})\Big] + \frac{e\hbar}{m_0 c}\big[\kappa\mathbf{J}\cdot\mathbf{B} + q_0\big(J_x^3 B_x + J_y^3 B_y + J_z^3 B_z\big)\big]. \quad (2)$$

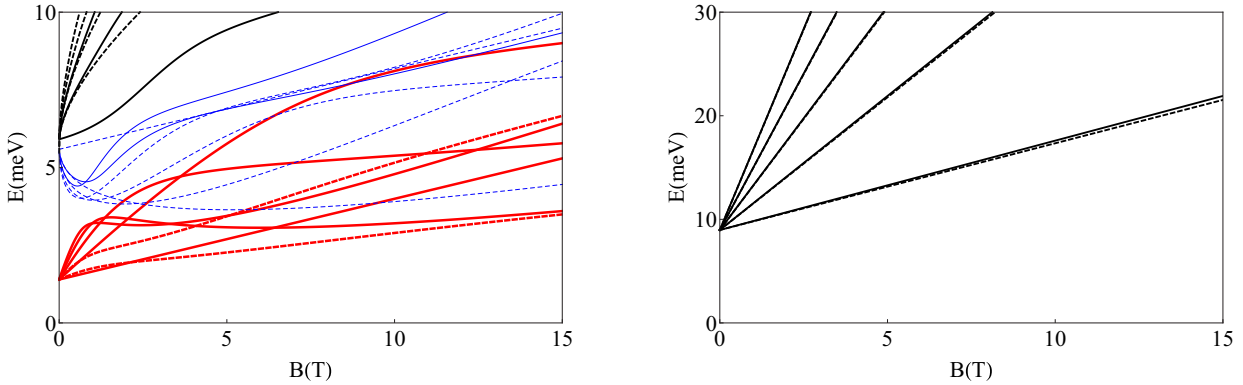

FIG. 2. (Color online) Comparison of the electron and hole spectra in a magnetic field. (Left) Fragment of the energy spectrum of GaAs holes with $n \leqslant 3$ in a quantum well of 250 Å for the two lowest size quantization levels of z-direction heavy holes, and one size quantization level of z-direction light holes; only the Luttinger Hamiltonian terms are included. (Right) Electron Landau levels with small Zeeman splitting in GaAs.

Throughout the paper, we will primarily express variables in dimensionless units: x, y, and z are the coordinates divided by the magnetic length ($\ell = \sqrt{\frac{\hbar c}{eB}}$), energies will be expressed in terms of the bare cyclotron energy $\hbar\omega_c = \frac{\hbar eB}{m_0 c}$, where m_0 is the bare electron mass, and the wave-vectors magnitude is made dimensionless by multiplying it with the magnetic length. Then the operators $\hat{k}_i$ are

$$\hat{k}_i = -i\partial_i + \frac{e\ell A_i}{\hbar c}, \quad i = x,y,z, \tag{3}$$

where $\vec{A}$ is the vector potential. They satisfy the commutation relationship $[\hat{k}_x,\hat{k}_y] = i$. Writing down Eq. (2) in a magnetic field with only symmetric combinations of $\{\hat{k}_i,\hat{k}_j\}$ and $\{J_i,J_j\}$, we skip the product of antisymmetric combinations of $[\hat{k}_i,\hat{k}_j]$ and $[J_i,J_j] = iJ_k\epsilon_{ijk}$, where ϵ_{ijk} is the unit antisymmetric tensor, arising from the zero magnetic field Luttinger Hamiltonian (1). Doing this, we follow the tradition [33] to account for such antisymmetric combinations in Eq. (2) through the term proportional to the constant κ, which therefore already describes not only the direct Zeeman effect, but also an additional contribution arising from the orbital motion. However, we will see that even the remaining symmetric orbital terms that couple the orbital angular momentum and momentum in Eq. (2) result in spin splitting of the hole states in a magnetic field.

The system of interest is the 2D hole gas in a GaAs/AlGaAs quantum well in the presence of a magnetic field $\vec{B} = -B\hat{z}$, $\hat{z}$ is a unit vector perpendicular to the plane of the well. We find the energy spectrum by solving the Schrödinger equation $H_0\Psi = E\Psi$ with the boundary conditions $\Psi(x,y,-w) = \Psi(x,y,w) = 0$, where $w = L/(2\ell)$, and use the Landau gauge $\vec{A} = (0,-Bx,0)$.

We shall make use of the bosonic operators [40]:

$$\hat{a}^\dagger = \frac{\hat{k}_x - i\hat{k}_y}{\sqrt{2}}, \quad \hat{a} = \frac{\hat{k}_x + i\hat{k}_y}{\sqrt{2}} \tag{4}$$

satisfying the commutation relation $[\hat{a},\hat{a}^\dagger] = 1$. They act as lowering and rising operators on wave functions of free electrons in a magnetic field:

$$\hat{a}u_{n,k_y}(x) = \sqrt{n}u_{n-1,k_y}(x), \tag{5}$$

$$\hat{a}^\dagger u_{n,k_y}(x) = \sqrt{n+1}u_{n+1,k_y}(x), \tag{6}$$

with

$$u_{n,k_y}(x) = \frac{i^n}{\sqrt{2^n n!\pi^{\frac{1}{2}}}} e^{-\frac{(x-k_y)^2}{2}} H_n(x-k_y), \tag{7}$$

where H_n is the n^{th} order Hermitte polynomial. In terms of these operators, the Luttinger Hamiltonian is

$$\begin{aligned}\hat{H} = &\left[\left(\gamma_1 + \frac{5\gamma_2}{2}\right)I - \gamma_2\{J_+,J_-\}\right]\left(\hat{a}^\dagger\hat{a} + \frac{1}{2}\right)\\ &+\left[\left(\frac{\gamma_1}{2} + \frac{5\gamma_2}{4}\right)I - \gamma_2 J_z^2\right]\hat{k}_z^2 - \kappa J_z - q_0 J_z^3\\ &-\sqrt{2}\gamma_3\hat{k}_z(\hat{a}^\dagger\{J_+,J_z\} + \hat{a}\{J_-,J_z\})\\ &-\frac{\gamma_2+\gamma_3}{4}[(\hat{a}^\dagger)^2 J_+^2 + \hat{a}^2 J_-^2]\\ &-\frac{\gamma_2-\gamma_3}{4}[(\hat{a}^\dagger)^2 J_-^2 + \hat{a}^2 J_+^2],\end{aligned} \tag{8}$$

where $J_\pm = J_x \pm iJ_y$. The first term contributes to the cyclotron motion, the second describes the z-direction motion, the next two are Zeeman-like terms, all of these resembling the corresponding features in electron systems. The fourth and fifth terms are nondiagonal terms describing coupling between spin and orbital motion. The fourth term couples the in-plane motion with motion in the direction of the quantization axis z, and, besides that, couples holes with light and heavy masses in the z direction. This is the term that results in mutual transformation of heavy and light holes upon reflection from the walls of the quantum well. As we have discussed in Introduction, this term results in a contribution to the kinetic energy of the same order of magnitude as the first term in (7), and essentially requires a nonpertubative treatment. We will also show that in a magnetic field the fourth term results in a sizable Zeemann splitting of holes. The fifth term couples the in-plane motion of holes with heavy mass in the z direction with angular momentum $\pm 3/2$ with the in-plane motion of the z-direction light holes with opposite sign angular momentum projection, $\mp 1/2$. The last term in Hamiltonian (7) contributes to the warping of the hole spectra. This term vanishes if $\gamma_2 = \gamma_3$. In what follows, we will be able to treat the first five terms "exactly" and the last term will be taken into account via (degenerate) perturbation theory. However, interesting enough, the fourth term in (8), which we use in analytical calculations, still contains the constant γ_3, and that will allow us to capture most of important anisotropic features, associated with the coupling of longitudinal and transverse motion in [001] grown quantum wells even before accounting for the last term. The only approximation used in our analytical approach is the form of the fifth term for the coupling of in-plane motion of different species of holes that contains the combination of constants $\gamma_2 + \gamma_3$ and the corresponding operator instead of the actual combination of operators, the rest of which is included in the small $\gamma_2 - \gamma_3$ term. In the axial approximation, which has been used by researchers to simplify numerical simulations of holes in a magnetic field [31,41], the last term is neglected. In this work, the axial approximation allows us to capture a significant part of the effects of anisotropy analytically, and numerical simulations account for the $\gamma_2 - \gamma_3$ term.

The eigenfunctions in the axial approximation are presented in the following form:

$$\Psi^{\{\alpha\}}(x,y,z) = \begin{pmatrix}\zeta_0^{\{\alpha\}}(z)u_{n,k_y}(x)\\ \zeta_1^{\{\alpha\}}(z)u_{n-1,k_y}(x)\\ \zeta_2^{\{\alpha\}}(z)u_{n-2,k_y}(x)\\ \zeta_3^{\{\alpha\}}(z)u_{n-3,k_y}(x)\end{pmatrix} e^{ik_y y}, \tag{9}$$

where $\zeta_i^{\{\alpha\}}(z)$'s are the envelope functions that have to be determined. Here, $\{\alpha\}$ denotes the set of quantum numbers that uniquely define the states: Landau level index n describing in-plane orbital motion, subband index describing spatial quantization along z direction, and parity symmetry with respect to reflection about the center-well plane, or spin. For the cases in which $n < 3$, the coefficients of negative index functions must be set to be zero. Then the Schrödinger equation with the general Hamiltonian (8) transforms effectively into an eigenfunction problem for the envelope functions,

$$\hat{H}_z\mathcal{Z}^{\{\alpha\}}(z) = E^{\{\alpha\}}\mathcal{Z}^{\{\alpha\}}(z), \tag{10}$$

where

$$\hat{H}_z = \begin{pmatrix} \frac{\hat{k}_z^2}{2m_h^z} + P_1 + Z_1 & \Gamma_1\hat{k}_z & A_1 & 0 \\ \Gamma_1\hat{k}_z & \frac{\hat{k}_z^2}{2m_l^z} + P_2 + Z_2 & 0 & A_2 \\ A_1 & 0 & \frac{\hat{k}_z^2}{2m_l^z} + P_2 - Z_2 & \Gamma_2\hat{k}_z \\ 0 & A_2 & \Gamma_2\hat{k}_z & \frac{\hat{k}_z^2}{2m_h^z} + P_1 - Z_1 \end{pmatrix}, \tag{11}$$

$P_1 = (\gamma_1 + \gamma_2)(n-1)$, $P_2 = (\gamma_1 - \gamma_2)(n-1)$, $m_h^z = (\gamma_1 - 2\gamma_2)^{-1}$, $m_l^z = (\gamma_1 + 2\gamma_2)^{-1}$, $A_1 = -\frac{\gamma_2+\gamma_3}{2}\sqrt{3n(n-1)}$, $A_2 = -\frac{\gamma_2+\gamma_3}{2}\sqrt{3(n-1)(n-2)}$, $\Gamma_1 = -\gamma_3\sqrt{6n}$, $\Gamma_2 = \gamma_3\sqrt{6(n-2)}$, $Z_1 = \frac{3(\gamma_1+\gamma_2)}{2} - \frac{3\kappa}{2} - \frac{27q_0}{8}$, $Z_2 = \frac{\gamma_1-\gamma_2}{2} - \frac{\kappa}{2} - \frac{q_0}{8}$, and

$$Z^{\{\alpha\}} = \begin{pmatrix} \zeta_0^{\{\alpha\}}(z) \\ \zeta_1^{\{\alpha\}}(z) \\ \zeta_2^{\{\alpha\}}(z) \\ \zeta_3^{\{\alpha\}}(z) \end{pmatrix}. \tag{12}$$

Solutions of Eq. (11) can be easily found. To see this, we present the envelope functions $\zeta(z)$ in the following form:

$$\zeta_i^{\{\alpha\}}(z) = \sum_{q_z} \lambda_{q_z,i}^{\{\alpha\}} e^{-iq_z z}. \tag{13}$$

For every eigenvalue E, there are eight wave vectors q_z that solve the secular equation involving H_z. In general, wave vectors q_z can be complex. It is easy to observe that if q_z is a solution of (11) then $-q_z$ is also a solution, with

$$\lambda_{-q_z,i}^{\{\alpha;p=1\}} = (-1)^i \lambda_{q_z,i}^{\{\alpha;p=1\}}, \tag{14}$$

$$\lambda_{-q_z,i}^{\{\alpha;p=-1\}} = (-1)^{i+1} \lambda_{q_z,i}^{\{\alpha;p=-1\}}. \tag{15}$$

This property allows for classification of states according to their parity with respect to reflection about the center plane of the quantum well $z = 0$ as even in the case (14) and odd in the case (15).

The imposition of the boundary conditions $\Psi^{\{\alpha\}}(x,y,w) = \Psi^{\{\alpha\}}(x,y,-w) = 0$ leads to another set of equations for the parameters λ:

$$\sum_{j=1}^{8} \lambda_{q_j,i}^{\{\alpha\}} e^{iq_j w} = 0, \quad \sum_{j=1}^{8} \lambda_{q_j,i}^{\{\alpha\}} e^{-iq_j w} = 0. \tag{16}$$

Equations (11) and (16) fully determine the spectrum. Using the parity property of Eqs. (14) and (15), we write a general form of the wave function as

$$\Psi^{n,k_y,p}(x,y,z) = \sum_{j=1}^{4} \begin{pmatrix} \lambda_{q_j,0}^{n,p}(e^{iq_j z} + pe^{-iq_j z})u_{n,k_y}(x) \\ \lambda_{q_j,1}^{n,p}(e^{iq_j z} - pe^{-iq_j z})u_{n-1,k_y}(x) \\ \lambda_{q_j,2}^{n,p}(e^{iq_j z} + pe^{-iq_j z})u_{n-2,k_y}(x) \\ \lambda_{q_j,3}^{n,p}(e^{iq_j z} - pe^{-iq_j z})u_{n-3,k_y}(x) \end{pmatrix} e^{ik_y y}. \tag{17}$$

We see indeed from Eq. (17) that there are no states characterized by a single standing wave in the z direction, except the case of $n = 0$. All other states contain two standing waves corresponding to holes with light and heavy masses in the $z$direction. This is the consequence of reflection of holes off the boundaries of the quantum well under oblique incidence, Fig. 1. Heavy holes are transformed into a combination of heavy and light holes, and light holes are transformed into a combination of light and heavy holes, so that there are no longer "pure" states [42]. This is a very important difference from the electronic spectra, where a single standing wave characterizes the $z$direction of motion perpendicular to the 2D plane. The importance of Eq. (17) is that it takes into account the mutual transformation of carriers with heavy and light masses in the $z$direction nonperturbatively, in the presence of a quantizing magnetic field.

III. SEMICLASSICAL SOLUTION

The Shrödinger equation for holes in a magnetic field is generally an infinite dimensional system of matrix equations. A general solution of this equation can only be found numerically. However, in the "semiclassical" limit, which will be precisely defined below, an analytical approach is possible. The Hamiltonian matrix can be divided into "time-symmetric" and "time-antisymmetric" parts [43]. In the space of 4×4 matrices, the time-reversal symmetric basis set is made of the identity matrix I, matices J_i^2, and $\{J_i, J_{\pm 1}\}$, while the matrices J_i, $\{J_i, J_{i+1}^2 - J_{i+2}^2\}$, J_i^3, and $\frac{1}{2}(J_x J_y J_z + J_z J_y J_x)$ make the time-reversal antisymmetric counterpart.

The time-reversal symmetric part of the Hamiltonian matrix is

$$H_s = \begin{pmatrix} \frac{\hat{k}_z^2}{2m_h^z} + P_1 & -\Gamma_s\hat{k}_z & A_s & 0 \\ -\Gamma_s\hat{k}_z & \frac{\hat{k}_z^2}{2m_l^z} + P_2 & 0 & A_s \\ A_s & 0 & \frac{\hat{k}_z^2}{2m_l^z} + P_2 & \Gamma_s\hat{k}_z \\ 0 & A_s & \Gamma_s\hat{k}_z & \frac{\hat{k}_z^2}{2m_h^z} + P_1 \end{pmatrix}, \tag{18}$$

where $A_s = (A_1 + A_2)/2$ and $\Gamma_s = (\Gamma_2 - \Gamma_1)/2$.

The antisymmetric part is

$$H_a = \begin{pmatrix} Z_1 & \Gamma_a\hat{k}_z & A_a & 0 \\ \Gamma_a\hat{k}_z & Z_2 & 0 & -A_a \\ A_a & 0 & -Z_2 & \Gamma_a\hat{k}_z \\ 0 & -A_a & \Gamma_a\hat{k}_z & -Z_1 \end{pmatrix}, \tag{19}$$

where $A_a = (A_1 - A_2)/2$ and $\Gamma_a = (\Gamma_1 + \Gamma_2)/2$.

We now observe that in the semiclassical limit ($n \gg 1$) matrix elements of the operator H_s describing the in-plane motion of holes are n times bigger than the matrix elements of the operator H_a. This fact allows one to treat the latter as a perturbation of the former.

A. Solution of the symmetric problem

We first analyze the Schrödinger equation generated by the symmetric part H_s of the Hamiltonian (18). We notice that each eigenenergy is realized by four values of the wave vector q_z which will be denoted by $\pm q_h$ and $\pm q_l$. We will call them heavy- and light-hole wave vectors, although, when warping of the energy surface is considered, it can happen that all q_z correspond to the bulk heavy hole band. Wave numbers q_l and q_h are such that $|q_l|\langle|q_h|$. Formally, the dependence of eigenvalues of the Hamiltonian (18) on q_z wave vectors can be written as

$$E_0^{n,\pm}(q_z)=\gamma_1\left(\frac{q_z^2}{2}+n-1\right)\pm\frac{1}{4}\sqrt{3\left[(\gamma_2+\gamma_3)^2(n-1)+8\gamma_3^2q_z^2\right](\sqrt{n}+\sqrt{n-2})^2+16\gamma_2^2\left(q_z^2-n+1\right)^2}. \tag{20}$$

In Eq. (20), the $\pm$ signs correspond to bulk heavy $(-)$ and light $(+)$ hole bands.

The eigenvectors of the Schrödinger equation will be determined by the Hopfield method [35,44], in which the z-envelope functions are expressed using the following basis set of eigenvectors of H_s:

$$\begin{pmatrix}\Gamma_s q_h\\ b_h\\ 0\\ -A_s\end{pmatrix}e^{-iq_hz},\quad\begin{pmatrix}-A_s\\ 0\\ b_h\\ -\Gamma_s q_h\end{pmatrix}e^{-iq_hz},\quad\begin{pmatrix}\Gamma_s q_l\\ b_l\\ 0\\ -A_s\end{pmatrix}e^{-iq_lz},\quad\begin{pmatrix}-A_s\\ 0\\ b_l\\ -\Gamma_s q_l\end{pmatrix}e^{-iq_lz}. \tag{21}$$

Four more vectors are obtained by replacing q_h by $-q_h$ and q_l by $-q_l$. In these expressions, $b_h=\frac{q_h^2}{2m_h^z}+P_1-E, b_l=\frac{q_h^2}{2m_h^z}+P_1-E$. The z-envelope functions are linear combinations of these vectors that correspond to standing wave solutions and are fully determined by imposing the boundary conditions. First, the boundary conditions are imposed on the $1/2$ and $-1/2$ components resulting in the even eigenfunctions

$$\mathcal{Z}_0^{n,k_y,1}(z)=N_e\begin{pmatrix}-A_s\left[\cos(q_hz)-\frac{b_h}{b_l}\frac{\cos(q_hw)}{\cos(q_lw)}\cos(q_lz)\right]+\alpha_e\Gamma_s\left[q_h\cos(q_hz)-q_l\frac{b_h}{b_l}\frac{\sin(q_hw)}{\sin(q_lw)}\cos(q_lz)\right]\\ i\alpha_eb_h\left[\sin(q_hz)-\frac{\sin(q_hw)}{\sin(q_lw)}\sin(q_lz)\right]\\ b_h\left[\cos(q_hz)-\frac{\cos(q_hw)}{\cos(q_lw)}\cos(q_lz)\right]\\ -i\Gamma_s\left[q_h\sin(q_hz)-q_l\frac{b_h}{b_l}\frac{\cos(q_hw)}{\cos(q_lw)}\sin(q_lz)\right]-i\alpha_eA_s\left[\sin(q_hz)-\frac{b_h}{b_l}\frac{\sin(q_hw)}{\sin(q_lw)}\sin(q_lz)\right]\end{pmatrix}, \tag{22}$$

and the odd eigenfunctions

$$\mathcal{Z}_0^{n,k_y,-1}(z)=N_o\begin{pmatrix}-iA_s\left[\sin(q_hz)-\frac{b_h}{b_l}\frac{\sin(q_hw)}{\sin(q_lw)}\sin(q_lz)\right]+i\alpha_o\Gamma_s\left[q_h\sin(q_hz)-q_l\frac{b_h}{b_l}\frac{\cos(q_hw)}{\cos(q_lw)}\sin(q_lz)\right]\\ \alpha_ob_h\left[\cos(q_hz)-\frac{\cos(q_hw)}{\cos(q_lw)}\cos(q_lz)\right]\\ ib_h\left[\sin(q_hz)-\frac{\sin(q_hw)}{\sin(q_lw)}\sin(q_lz)\right]\\ -\Gamma_s\left[q_h\cos(q_hz)-q_l\frac{b_h}{b_l}\frac{\sin(q_hw)}{\sin(q_lw)}\cos(q_lz)\right]-\alpha_oA_s\left[\cos(q_hz)-\frac{b_h}{b_l}\frac{\cos(q_hw)}{\cos(q_lw)}\cos(q_lz)\right]\end{pmatrix}. \tag{23}$$

The wave vectors q_l and q_h and constants α_e and α_o will be calculated using the remaining boundary conditions on $\pm3/2$ components, while the normalization conditions will provide N_e and N_o.

From the boundary conditions invoked for $3/2$ and $-3/2$ spin components of the eigenvectors it follows that

$$\tau^2-\left[\frac{b_l}{b_h}\frac{A_s^2}{\Gamma_s^2q_h^2}\left(1-\frac{b_h}{b_l}\right)^2+\frac{b_l}{b_h}+\frac{b_hq_l^2}{b_lq_h^2}\right]\tau+\frac{q_l^2}{q_h^2}=0, \tag{24}$$

where

$$\tau=\frac{q_l\tan(q_hw)}{q_h\tan(q_lw)}. \tag{25}$$

Equations (24) and (25) together with the dependence of the energy on the q_z wave vectors of Eq. (20) determine q_h and q_l and thereby the energy spectrum. In the presence of a magnetic field, q_h and q_l depend on its value and on the Landau index n describing the in-plane motion of the holes, due to Luttinger spin-orbit coupling. Also from the boundary conditions we determine the α's:

$$\alpha_e=\frac{A_s}{\Gamma_sq_h}\frac{b_l-b_h}{b_l-b_h\tau}, \tag{26}$$

$$\alpha_o=\frac{\Gamma_sq_h}{A_s}\frac{b_h\tau-b_l}{b_l-b_h}. \tag{27}$$

The evaluation of the normalization constants N_e and N_o is straightforward. Introducing the notation

$$c_c \equiv \frac{1}{w}\int_{-w}^{w} dz \left|\cos(q_h z) - \frac{\cos(q_h w)}{\cos(q_l w)}\cos(q_l z)\right|^2 = \mathrm{sinhc}(2\Im m q_h w) + \mathrm{sinc}(2\Re e q_h w)$$
$$- 2\Re e\left(\frac{\cos(q_h w)}{\cos(q_l w)}\{\mathrm{sinc}[(q_h^* - q_l)w] + \mathrm{sinc}[(q_h^* + q_l)w]\}\right) + \left|\frac{\cos(q_h w)}{\cos(q_l w)}\right|^2 [\mathrm{sinhc}(2\Im m q_l w) + \mathrm{sinc}(2\Re e q_l w)], \quad (28)$$

$$c_s \equiv \frac{1}{w}\int_{-w}^{w} dz \left|\sin(q_h z) - \frac{\sin(q_h w)}{\sin(q_l w)}\sin(q_l z)\right|^2$$
$$= \mathrm{sinhc}\,(2\Im m q_h w) - \mathrm{sinc}(2\Re e q_h w) - 2\Re e\left\{\frac{\sin(q_h w)}{\sin(q_l w)}\left\{\mathrm{sinc}\left[\left(q_h^* - q_l\right)w\right] - \mathrm{sinc}\left[\left(q_h^* + q_l\right)w\right]\right\}\right\}$$
$$+ \left|\frac{\sin(q_h w)}{\sin(q_l w)}\right|^2 [\mathrm{sinhc}\,(2\Im m q_l w) - \mathrm{sinc}(2\Re e q_l w)]\,, \quad (29)$$

$$\eta \equiv 1 + \left|\frac{b_l - b_h\tau}{A_s(\tau - 1)}\right|^2 + \frac{c_s}{c_c}\left|\frac{b_l - b_h}{\Gamma_s q_h(\tau - 1)}\right|^2\left[1 + \left|\frac{A_s}{b_h}\right|^2\left|1 + \left(\frac{\Gamma_s q_h}{A_s}\right)^2\frac{b_l - b_h\tau}{b_l - bh}\right|^2\right], \quad (30)$$

we find that the wave functions of the time-symmetric Hamiltonian are given by

$$\Psi_0^{n,k_y,1}(x,y,z) = \frac{1}{\sqrt{wc_c\eta}}e^{ik_y y}\begin{pmatrix} \left[\cos(q_h z) - \frac{\cos(q_h w)}{\cos(q_l w)}\cos(q_l z)\right]u_n(x) \\ i\frac{b_l - b_h}{\Gamma_s q_h(\tau-1)}\left[\sin(q_h z) - \frac{\sin(q_h w)}{\sin(q_l w)}\sin(q_l z)\right]u_{n-1}(x) \\ \frac{b_l - b_h\tau}{A_s(\tau-1)}\left[\cos(q_h z) - \frac{\cos(q_h w)}{\cos(q_l w)}\cos(q_l z)\right]u_{n-2}(x) \\ -i\frac{b_l - b_h}{\Gamma_s q_h(\tau-1)}\frac{A_s}{b_h}\left[1 + \left(\frac{\Gamma_s q_h}{A_s}\right)^2\frac{b_l - b_h\tau}{b_l - b_h}\right]\left[\sin(q_h z) - \frac{\sin(q_h w)}{\sin(q_l w)}\sin(q_l z)\right]u_{n-3}(x) \end{pmatrix}, \quad (31)$$

and

$$\Psi_0^{n,k_y,-1}(x,y,z) = \frac{1}{\sqrt{wc_c\eta}}e^{ik_y y}\begin{pmatrix} i\frac{b_l - b_h}{\Gamma_s q_h(\tau-1)}\frac{A_s}{b_h}\left[1 + \left(\frac{\Gamma_s q_h}{A_s}\right)^2\frac{b_l - b_h\tau}{b_l - b_h}\right]\left[\sin(q_h z) - \frac{\sin(q_h w)}{\sin(q_l w)}\sin(q_l z)\right]u_n(x) \\ \frac{b_l - b_h\tau}{A_s(\tau-1)}\left[\cos(q_h z) - \frac{\cos(q_h w)}{\cos(q_l w)}\cos(q_l z)\right]u_{n-1}(x) \\ -i\frac{b_l - b_h}{\Gamma_s q_h(\tau-1)}\left[\sin(q_h z) - \frac{\sin(q_h w)}{\sin(q_l w)}\sin(q_l z)\right]u_{n-2}(x) \\ \left[\cos(q_h z) - \frac{\cos(q_h w)}{\cos(q_l w)}\cos(q_l z)\right]u_{n-3}(x) \end{pmatrix}. \quad (32)$$

These wave functions largely represent the effect of mutual transformation of the states characterized by the z components of the wave vectors describing heavy and light holes, as the physical picture of Fig. 1 suggests. However, despite that the symmetric Hamiltonian H_s includes the effects of spin-orbit interactions and the effects of an external magnetic field, by its construction, it still gives states that are Kramers-degenerate. Removal of the Kramers degeneracy takes place due to the time-reversal asymmetric part H_a, which gives the Zeemann splitting of hole states.

B. Antisymmetric Hamiltonian and removal of Kramers degeneracy

In the semiclassical approximation, the antisymmetric Hamiltonian H_a is considered as a perturbation. The z-envelope functions given by Eqs. (31) and (32) satisfy

$$\left\langle \mathcal{Z}_0^{n,k_y,1}(z)\middle|H_a\middle|\mathcal{Z}_0^{n,k_y,1}(z)\right\rangle = -\left\langle \mathcal{Z}_0^{n,k_y,-1}(z)\middle|H_a\middle|\mathcal{Z}_0^{n,k_y,-1}(z)\right\rangle, \quad (33)$$

and as a consequence the (perturbed) energies of the even and odd states can be written as $E_e^n = E_0^n + \Delta E$ and $E_o^n = E_0^n - \Delta E$, where

$$\Delta E = \frac{2\Gamma_a}{\Gamma_s c_c \eta}\Re e\left\{c_\tau\left[\frac{b_l - b_h}{\tau - 1} - \frac{b_l - b_h}{b_h}\frac{b_l^* - b_h^*\tau^*}{|\tau - 1|^2} - \frac{1}{b_h}\left(\frac{\Gamma_s q_h}{A_s}\right)^2\left|\frac{b_l - b_h\tau}{\tau - 1}\right|^2\right]\right\}$$
$$+ \frac{c_s}{c_c\eta}\left|\frac{b_l - b_h}{\Gamma_s q_h(\tau - 1)}\right|^2\left\{Z_2 + 2A_a A_s\Re e\left[\frac{1}{b_h} + \left(\frac{\Gamma_s q_h}{A_s}\right)^2\frac{b_l - b_h\tau}{b_h(b_l - b_h)}\right] - Z_1\frac{A_s^2}{|b_h|^2}\left|1 + \left(\frac{\Gamma_s q_h}{A_s}\right)^2\frac{b_l - b_h\tau}{b_l - b_h}\right|^2\right\}$$
$$+ \frac{1}{\eta}\left[Z_1 + 2\frac{A_a}{A_s}\Re e\left(\frac{b_l - b_h\tau}{\tau - 1}\right) - \frac{Z_2}{A_s^2}\left|\frac{b_l - b_h\tau}{\tau - 1}\right|^2\right], \quad (34)$$

with

$$c_\tau \equiv \frac{1}{w}\int_{-w}^{w} dz\left[\cos(q_h^* z) - \frac{\cos(q_h^* w)}{\cos(q_l^* w)}\cos(q_l^* z)\right]\left[\cos(q_h z) - \tau\frac{\cos(q_h w)}{\cos(q_l w)}\cos(q_l z)\right]$$

$$= \mathrm{sinhc}(2\Im m q_h w) + \mathrm{sinc}(2\Re e q_h w) - \tau\frac{\cos(q_h w)}{\cos(q_l w)}\{\mathrm{sinc}[(q_h^* - q_l)w] + \mathrm{sinc}[(q_h^* + q_l)w]\}$$

$$- \frac{\cos(q_h^* w)}{\cos(q_l^* w)}\{\mathrm{sinc}[(q_h - q_l^*)w] + \mathrm{sinc}[(q_h + q_l^*)w]\} + \tau\left|\frac{\cos(q_h w)}{\cos(q_l w)}\right|^2[\mathrm{sinhc}(2\Im m q_l w) + \mathrm{sinc}(2\Re e q_l w)]. \quad (35)$$

There is no change in the wave functions at first order in perturbation theory as $\langle(\mathcal{Z}_0^{n,k_y,1}(z))|H_a|\mathcal{Z}_0^{n,k_y,-1}(z)\rangle = 0$.

C. Analytic solution in semiclassical approximation

Even when the semiclassical approximation is used, the calculations are rather complex due to the strong coupling between the z-direction motion and the cyclotron degrees of freedom. Generally, the transcendental Eqs. (24) and (25) cannot be solved analytically. However, an approximate solution with high accuracy is possible, if the energy associated with motion in the z direction, i.e., the size quantization energy is much larger than the cyclotron in-plane energy, $q_z^2 \gg n \gg 1$. That is the case of strong size quantization, when the quantum well width is much smaller than the magnetic length, e.g., $w \ll 1$. This gives a small parameter for the perturbative expansion, so that the wave vector is expanded in a series of dimensionless w as

$$q_z = \frac{p\pi r}{2w} + w\delta, \quad (36)$$

where r is an integer and q_z can be either the heavy or light hole z-direction wave number. Obviously, the first term in Eq. (36) (zeroth-order approximation) gives a wave number similar to that describing electrons in an infinite rectangular quantum well. However, the eigenstates of H_s contain both light and heavy wave numbers, though only one of them is close to usual $\pi r/(2w)$, and both depend on the magnetic field and the Landau level index.

The coefficient δ, which describes the dependence of the wave numbers on the Landau level index, is calculated as follows. The energy given by Eq. (20) can be expanded when $q_z^2 \gg n \gg 1$ for heavy and light holes as

$$E_h^n \approx \frac{q_z^2}{2m_h^z} + \left(\gamma_1 + \gamma_2 - \frac{3\gamma_3^2}{\gamma_2}\right)(n-1), \quad (37)$$

$$E_l^n \approx \frac{q_z^2}{2m_l^z} + \left(\gamma_1 - \gamma_2 + \frac{3\gamma_3^2}{\gamma_2}\right)(n-1). \quad (38)$$

We emphasize that the terms containing q_z here have a hidden contribution to the cyclotron energy of the holes in two dimensions because of the q_z's dependence on the magnetic field and Landau level index. Using these expressions for energy and the expansion of the q_z wave vector from Eq. (36), one can solve Eq. (24) and obtain the equation for the quantity τ of a given state. The expansion for τ in powers of w can also be obtained by replacing the wave vectors in Eq. (25). Comparing the leading order terms in w of these two expressions for τ, we find the coefficient δ. The details of this procedure are explained in Appendix A. The resulting expression for the wave numbers is given by

$$\delta = \frac{6(-1)^{r+1}n}{r^2\pi^2}\frac{\gamma_3^2}{\gamma_2^2}\sqrt{\left(\frac{\gamma_1+2\gamma_2}{\gamma_1-2\gamma_2}\right)^s} \times\left\{\tan\left[\frac{r\pi}{2}\sqrt{\left(\frac{\gamma_1-2\gamma_2}{\gamma_1+2\gamma_2}\right)^s}\right]\right\}^{(-1)^r} \quad (39)$$

where $s=1$ corresponds to heavy holes and $s=-1$ to light holes.

In the zeroth-order approximation, the eigenvectors of Eq. (31) become the up and down spinors ${}^T(u_n\zeta_0(z),0,0,0)$ and ${}^T(0,0,0,u_{n-3}\zeta_3(z))$ for heavy-hole bands and ${}^T(0,u_{n-1}\zeta_1(z),0,0)$ and ${}^T(0,0,u_{n-2}\zeta_2(z),0)$ for light-hole bands. We will see that the in-plane (cyclotron) masses characterizing these states coincide with Nedorezov effective masses [34] in zero magnetic field, which are the correct in-plane effective masses accounting for the effects of the mutual transformation of heavy and light holes.

IV. ENERGY SPECTRA: NUMERICAL RESULTS

In the general case, and most notably for low lying levels, the antisymmetric part H_a is comparable to the symmetric part H_s, and a perturbative procedure does not work. This regime is examined through a numerical solution of the Schrödinger equation with the Luttinger Hamiltonian (8) in a quantum well which we now discuss. The first three subbands of the energy spectrum (the two lowest heavy hole and the lowest light hole band) are presented in Fig. 3. We see indeed that the spectra do not have a fanlike shape characteristic of electron systems. The levels bend and cross as the magnetic field increases. As a consequence, the Landau level number n does not describe the ordering of levels. We observe that there is a large energy separation between symmetric and antisymmetric states, a clear signature of a gigantic intrinsic SO coupling. As we shall see in Sec. VII, some crossings could become anticrossings in the presence of Dresselhaus spin-orbit coupling. We will also show elsewhere [45] that some of the crossings could become anticrossings due to hole-hole interactions.

We find that the ground state of the holes is characterized by a crossing between the 0-even parity and 3-odd parity state, the former being the ground state at relatively small fields, while the latter taking over at large fields. Level crossings are of critical importance, especially since novel fractional quantum Hall states with even denominator have been shown to appear at such crossings in recent experiments [46,47]. We note that experimental observation of Landau levels for holes in photoluminescence measurements also reveals crossings [48].

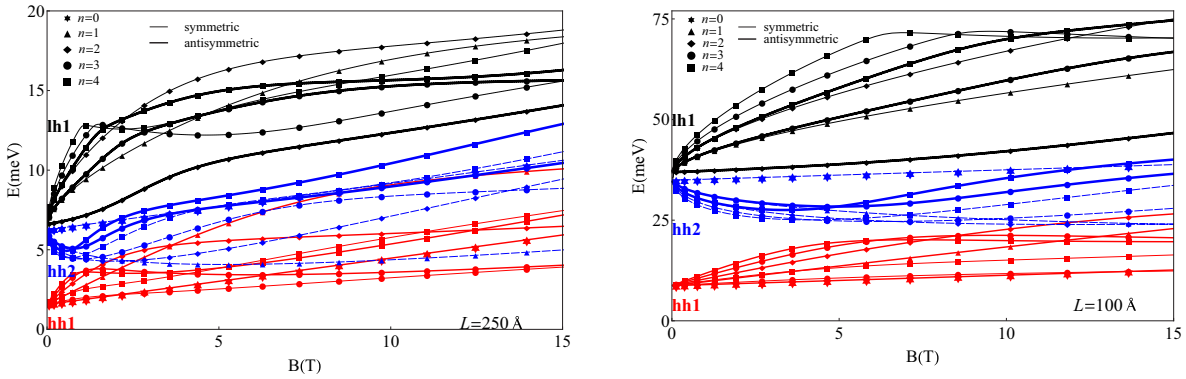

FIG. 3. (Color online) Energy spectrum of GaAs holes with $n \leqslant 3$ in a quantum well of 250 Å (left) and 100 Å (right).

For excited states, one interesting feature that we observe is almost a degeneracy between the second z-direction heavy hole state and the first z-direction light hole state at small magnetic fields. This effect occurs because the z-direction effective mass of light holes $1/(\gamma_1 + 2\gamma_2) = 0.091$ is roughly four times smaller than the mass of heavy holes $1/(\gamma_1 - 2\gamma_2) = 0.38$. As the magnetic field increases, these states strongly hybridize. This makes the range of applicability of the semiclassical approximation even narrower.

A comparison between the numerical and semiclassical solutions shows a very good agreement for large Landau level indices, as expected. Such comparisons are presented for $n = 10$ and 20 in the lowest three subbands in Figs. 4–6. The semiclassical solution takes into account the time-antisymmetric perturbation, however, both the numerical and semiclassical solutions are in the axial approximation for this section, i.e., the last term in Eq. (8) is excluded. We observe that the comparison shows the semiclassical approximation to work better for $n = 20$ as one expects for the semiclassical theory. The shape of these curves includes a linear regime at a small magnetic field and large n (also the magnetic length should be much larger than the width of the quantum well). For large n here, the hole energy spectrum shows a fanlike diagram and no crossings, making the hole spectrum resemble the electronic spectra in a magnetic field. At larger magnetic fields (or small n), the energy curves for holes bend. These are the range of fields where crossings occur.

The ordering of the levels and the corresponding resonant transitions that are used to measure hole parameters in the perturbative semiclassical regime are shown in Fig. 7. Only in this regime can holes be described in a way similar to electrons. However, as we shall discuss in the next section, experiments are conducted largely outside of this range of magnetic fields.

V. CYCLOTRON MASS

Numerous experiments study the effective mass of holes in GaAs based heterostructures, including recent works [31,49–51]. The experiments detect the microwave magnetoplasma resonance. Unlike electron systems, the data for holes show two distinct sets of masses, with values depending on the magnetic field, well width, and hole density. The physical picture is totally different from the case of the electron liquid in GaAs that exhibits one cyclotron mass.

Theoretically the cyclotron mass can be defined, in terms of quantized energy levels, as the inverse of the energy distance between the highest (partially) occupied Landau level and the lowest empty (or highest filled LL) whose indices differ by 1 and have the same parity, as follows from the cyclotron resonance theory [52]. Absorption of radiation (its electric field component) is due to transitions between these levels. Accordingly, in quantum cyclotron resonance,

$$m_p = \pm \frac{1}{E^{n\pm1,p} - E^{n,p}}. \tag{40}$$

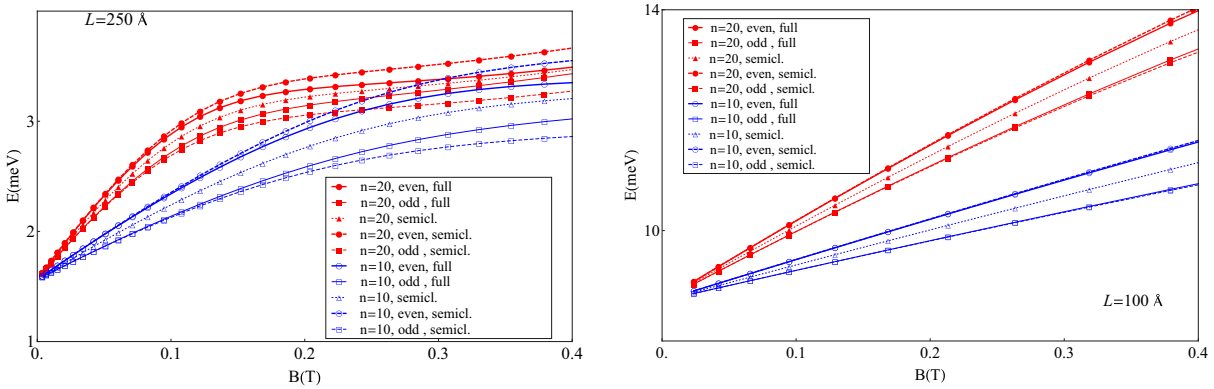

FIG. 4. (Color online) Comparison between the numerically evaluated spectrum and the semiclassical values of the lowest heavy hole band for $n = 10$ and 20. The quantum well width is 250 Å (left) and 100 Å (right).

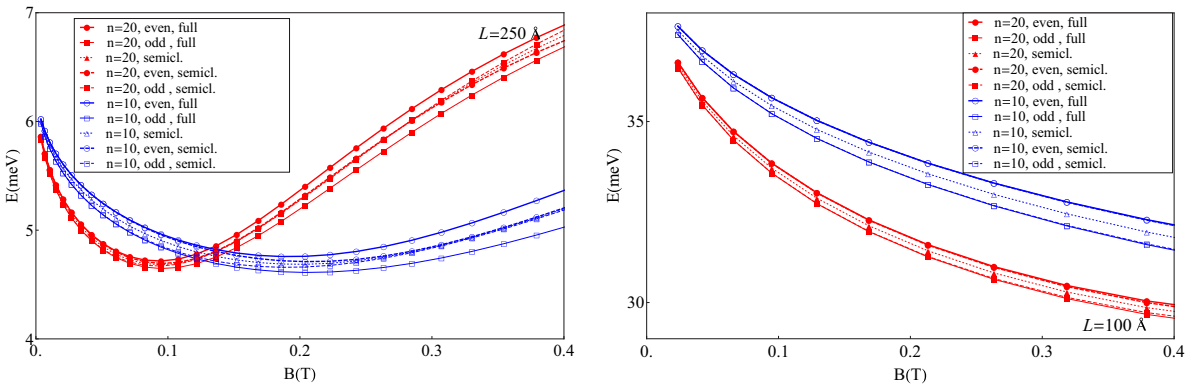

FIG. 5. (Color online) Comparison between the numerically evaluated spectrum and the semiclassical values of the second heavy-hole band for $n = 10$ and 20. The quantum well width is 250 Å (left) and 100 Å (right).

It is well known that even for the electron spectrum, besides cyclotron transitions and electron spin resonance transitions (the latter due to the magnetic field component of the radiation), there are also electric-field induced combined resonance transitions [53]. However, all these transitions can be distinguished based on the intensity of the lines and the polarization of the radiation, and it is reasonable to assume that it is indeed the effective mass that is measured by the energy of the principal cyclotron transition (40). Our theoretical analysis of the hole spectra shows that the traditional meaning of effective mass is preserved only if the in-plane motion can be clearly separated from the other degrees of freedom, that is, spin and/or coupling to transverse motion. Such separation occurs in the semiclassical regime at $q_z\lambda \gg 1$. Using Eqs. (36) and (39), the parity independent effective mass of holes is

$$m_{\parallel} = \left(\gamma_1 + s\gamma_2 - s\frac{3\gamma_3^2}{\gamma_2}\right) - \frac{3(-1)^r}{r^2\pi^2}\frac{\gamma_3^2}{\gamma_2^2}\sqrt{\left(\gamma_1^2 - 4\gamma_2^2\right)^s} \times \left\{\tan\left[\frac{r\pi}{2}\sqrt{\left(\frac{\gamma_1 - 2\gamma_2}{\gamma_1 + 2\gamma_2}\right)^s}\right]\right\}^{(-1)^r}, \quad (41)$$

where $s = 1$ corresponds to heavy holes and $s = -1$ to light holes, and r labels the subbands. This semiclassic value is, as expected, precisely the result obtained in the absence of magnetic field by Nedorezov [34,54], and constitutes the in-plane effective mass of holes. The effective mass for holes with heavy (light) mass in the z direction in Eq. (41) contains the contribution in round brackets, which, for $\gamma_3 = \gamma_2$, coincides with the bulk heavy (light) hole mass in the axial approximation. Our procedure treats nonperturbatively the γ_3 term in Eq. (8), which describes coupling of heavy and light holes and coupling of z direction and in-plane motion, thereby allowing us largely to take into account the effects of anisotropy. The last term in the expression for the cyclotron mass (41) is the contribution from the size quantization that depends on the size quantization level quantum number but is independent of the well width [54]. In a magnetic field, this cyclotron mass is independent of the well width in the range of applicability of Eq. (41), $\lambda q_z, \lambda/w \gg 1$, in much the same way as the expression for the effective mass in zero field is independent of the well width at $q_z \gg k_{\text{in-plane}}$.

Interpreting cyclotron resonances outside the regime $\lambda q_z, \lambda/w \gg 1$, $n \gg 1$ is a challenging task, because they depend of the actual details of the experimental setting. Unlike the electron case, the spectra are not fanlike, and the separation between levels changes with both well width and magnetic field. As the Fermi level goes through various levels with different Landau indices, the cyclotron mass seemingly changes its value. However, as we shall see, the observed cyclotron mass is defined by the absorption of energy, and as a result of several transitions contributing to the signal, abrupt changes in cyclotron mass may occur only at crossings. We also note that, in general, the cyclotron mass for holes is not equal to the effective mass (band mass). While for metals this fact is

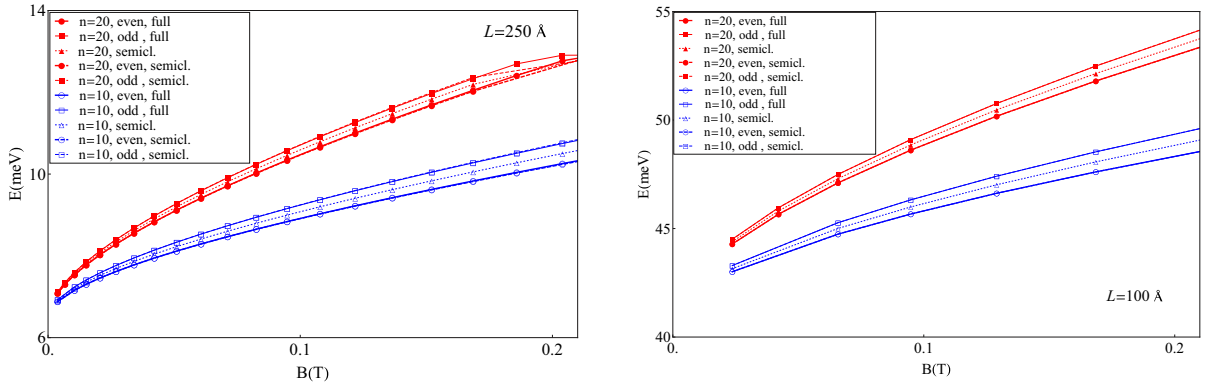

FIG. 6. (Color online) Comparison between the numerically evaluated spectrum and the semiclassical values of the lowest light hole band for $n = 10$ and 20. The quantum well width is 250 Å (left) and 100 Å (right).

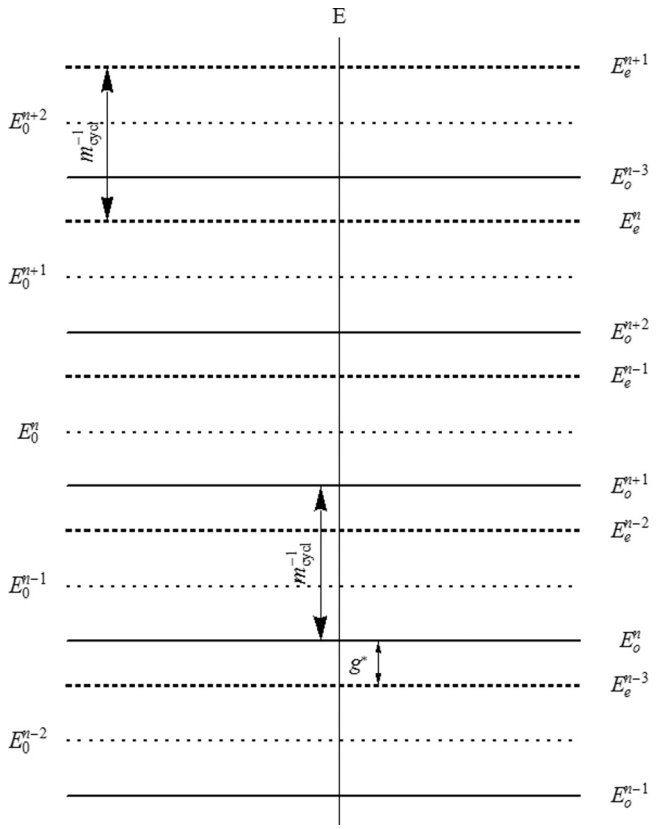

FIG. 7. Energy spectrum in the semiclassical limit for the lowest band of heavy holes. The dotted lines represent the levels obtained from the time-symmetric Hamiltonian of Eq. (18), dashed lines represent the even states, solid lines are the odd states. The arrows represent the cyclotron and spin resonance transitions measuring the cyclotron mass and effective g factor, respectively.

related to the topology of Fermi surfaces, for semiconductors with a low density of charge carriers, the situation is unusual.

Let us consider first the range of magnetic fields, in which there are no level crossing. A cyclotron resonance can occur for a transition between nth partially occupied level and the $n+1$ or $n-1$ level with the same parity. As levels are not equidistant, these are two different resonances. Our calculations indicate that they are close to each other and hence inseparable given the experimental accuracy and energy level broadening. When the two resonant lines are present, the "measured" cyclotron frequency is a weighted average of the individual ones, the weights being the intensities of the lines. If n is partially filled, the intensity of the $n \to (n+1)$ transition is proportional to the number of holes on the nth level (i.e., to the fractional part of filling factor, ν^*), while the intensity of the $(n-1) \to n$ transition is proportional to the number of empty states on the nth level $(1-\nu^*)$. As a consequence, the effective mass is continuous in changes in the integer part of the filling factor. To see this, let us consider, for example, the level n with odd parity, which is partially filled and is located between the levels p and $p+1$, both of even parity. The possible cyclotron transitions are then $(n,\text{odd}) \to (n+1,\text{odd})$ and $(n-1,\text{odd}) \to (n,\text{odd})$ and $(p,\text{even}) \to (p+1,\text{even})$. As the level n-odd is filling up, the intensity of the lines corresponding to the transition $(n-1,\text{odd}) \to (n,\text{odd})$ decreases, eventually becoming zero when the level n is completely filled. The transition $(n,\text{odd}) \to (n+1,\text{odd})$ becomes stronger as the level (n,odd) is being filled up, eventually becoming the only allowed transition between even states when the level is filled. Such "measured" frequency, becomes closer to the one corresponding to $(n,\text{odd}) \to (n+1,\text{odd})$ when the level (n,odd) is gradually filled up. Thus in this case there is no discontinuity in the odd state mass. The argument is the same for the even state mass. However, there exist discontinuities in the cyclotron mass from level crossings in the hole spectrum. This analysis explains the experimental observations in Ref. [31].

Calculated cyclotron masses for the set of magnetic quantized levels from the lowest heavy-hole subband are plotted in Figs. 8 and 9. Numerical calculations of the cyclotron mass were performed assuming that the quantum well of GaAs is embedded in $Al_{0.24}GaAs_{0.76}$ substrate, and the finite height of the quantum well (valence band offset) was taken into account. We have also assumed that the charge carriers originate from a single doping layer resulting in an electric field of 10^3V/cm across the well (circles). We are not interested here in a self-consistent calculation of the whole heterostructure, and will consider both Hartree and exchange hole interactions elsewhere [45], and take this value of the electric field for the sake of illustration irrespective of the density of holes. Squares in the figures represent the values of the cyclotron masses for the infinite rectangular well. It is immediately seen that the masses of the symmetric (red lines) and antisymmetric states (blue ones) are different. This is due to the bending of levels, that effectively acts as level repulsion between states with the same n. This sends odd levels to lower energies and smaller separations, while the symmetric even states are higher levels. This effect is more pronounced in wider wells. Higher concentration of holes leads to higher Landau indices for the partially filled level, making $w^2 n > 1$, thus taking the system away from the $q_z^2 \gg n$ range of the semiclassical regime and resulting in higher cyclotron masses. The differences of the actual masses from their semiclassical values are further enhanced by the finite height of the well and the electric field. In sufficiently high electric field, one can expect rather large effective masses obtained in triangular quantum wells of structures with a single heteroboundary [27,29].

In order to get a better understanding of wide variations in the values of cyclotron mass, details of the data for the 250 Å wide quantum well with higher density of holes is presented in Fig. 10. There are six ranges of field, in which cyclotron mass shows a linear behavior, and there are discontinuities between these regions. At the left of the graph (region I), the filling factor is between 8 and 9, the partially filled level is characterized by $n = 7$, and it has odd parity. The highest occupied state with even parity in this range is characterized by $n = 3$. The symmetry-allowed cyclotron resonance transitions are (7, odd) $\to$ (8, odd), (6, odd) $\to$ (7, odd), and (3, even) $\to$ (4, even). The transition (6, odd) $\to$ (7, odd) becomes stronger with the increase of field while the transition (7, odd) $\to$ (8, odd) becomes weaker and is zero once the filling factor equals 8 . When magnetic field increases further, the filling factor is between 7 and 8 in the range II. The important feature is that at the boundary between I and II, levels 3 even and 7 odd cross. As a consequence, the partially filled level is 7 odd,

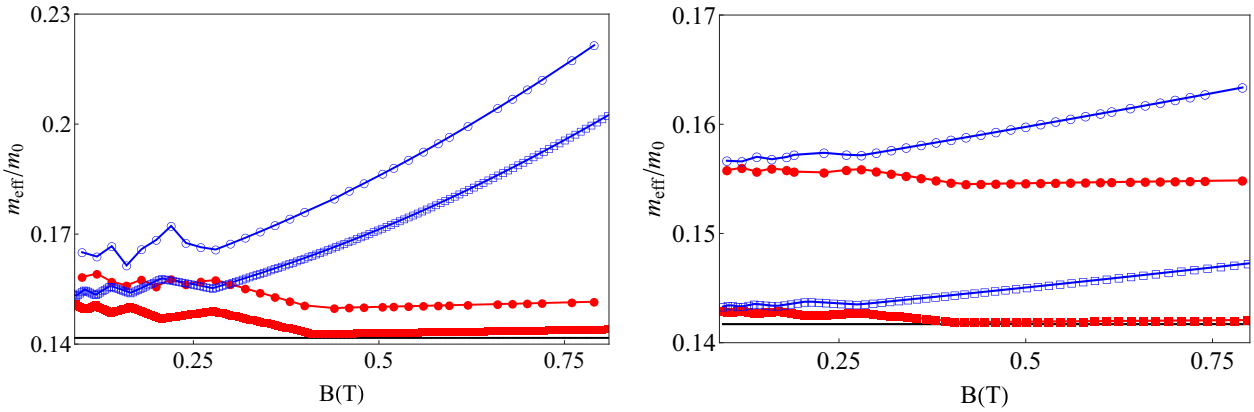

FIG. 8. (Color online) Cyclotron mass for the hole spectrum with crossings. The hole density is $2\times\ 10^{10}$ cm^{-2}. The red lines (solid symbols) represent the cyclotron mass corresponding to even parity states, while the blue lines (empty symbols) represent the mass describing odd states. Circles represent the cyclotron mass for a finite barrier well in an electric field of 10^3 V/cm, squares represent the cyclotron mass in an infinite rectangular quantum well. (Right) 250-Å well and (left) 100-Å well. The black line represents the semiclassical limit.

and the highest even state is characterized by $n = 2$, so that the only allowed transition is (2, even) $\rightarrow$ (3, even) . Because the levels are not equidistant, the transition with the biggest amplitude between odd parity levels at the boundary with region I is (7, odd) $\rightarrow$ (8, odd). The only allowed transition between even parity levels is (2, even)$\rightarrow$ (3, even). Both even and odd transitions disappear at the crossing when change in the value of magnetic field brings the system from range I into range II or from range II to range I, correspondingly. Therefore masses for both even and odd parity levels exhibit discontinuities. In region III, the filling factor is between 6 and 7 and the partially filled levels is $n = 6$ with odd parity while the highest even state is with $n = 2$. There is no change in effective mass here. In the region IV, the filling factor is between 5 and 6, the partially filled level is $n = 2$ with even parity and the highest filled odd state is $n = 5$. The boundary with region V corresponds to a crossing of 2-even and 6-odd, the later becoming the highest (partially) filled state. Both even and odd masses change. The filling factor becomes smaller than 5 in region VI and no discontinuity in effective mass occurs at the boundaries between these regions, because no crossings are present. These facts are summarized in Table I.

While discussing the cyclotron mass for holes, it is important to mention that as has been long appreciated [27,55], due to mixing of light and heavy carriers, the Kohn theorem [56], asserting that charge carrier interactions do not alter the cyclotron frequency, is no longer valid. In fact, a large effective $r_s \approx 3.5$ opens up the possibility that many-body corrections are significant. The masses we have calculated are generally in the range of values of masses observed experimentally. However, several experiments show considerably bigger masses in certain ranges of magnetic field [9,31,50,51,57,58]. In the single-particle picture, the only possible explanation of the ground state 2D hole mass exceeding $0.15m_0$ is related to holes being subject to a magnetic field away from the semiclassical regime. If the analysis of experiments indicates that the ground state mass of the holes exceeds the value $0.15m_0$ for the range of parameters corresponding to the semiclassical regime, the only possible explanation would be interaction effects. At this stage, we restrict our consideration to the single-particle picture.

VI. EFFECTIVE LANDÉ FACTOR

One of the most important questions in the hole spectra is spin splitting in the hole states, and the Landé or g factor.

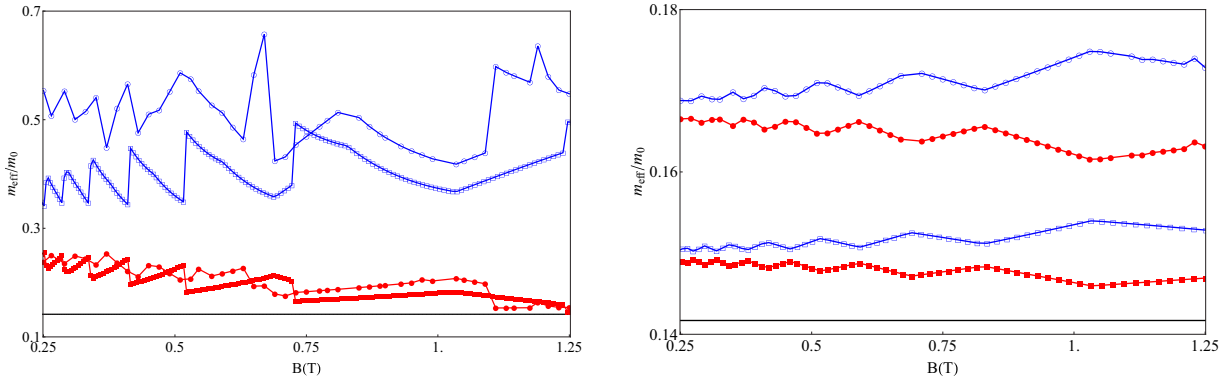

FIG. 9. (Color online) Cyclotron mass for the hole spectrum with crossings. The hole density is 10^{11} cm^{-2}. The red lines (solid symbols) represent the cyclotron mass corresponding to even states while the blue lines (empty symbols) represent the mass describing odd states. Circles represent the cyclotron mass for a finite barrier well in an electric field of 10^3 V/cm, squares represent the cyclotron mass in an infinite rectangular quantum well. (Right) 250-Å well and (left) 100-Å well. The black line represents the semiclassical limit.

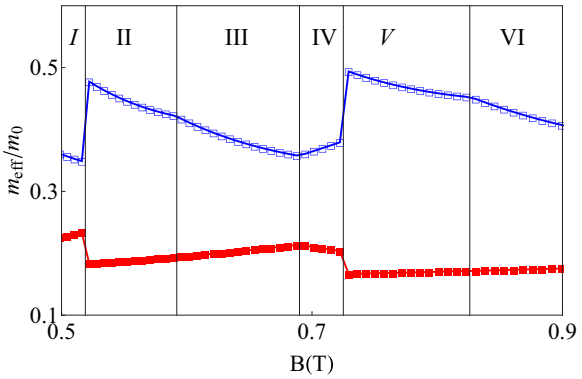

FIG. 10. (Color online) Detail of the cyclotron mass dependence on magnetic field for a hole density of 10^{11} cm^{-2} in a 250-Å-wide infinite rectangular quantum well. Red line (solid symbols) is even states and blue line (empty symbols) is odd states.

Over the past decade, numerous studies were devoted to possible application of hole systems to spintronic devices and quantum bits with strongly suppressed spin decoherence. The problem of the effective Landé factor in 2D hole systems has been investigated both theoretically and experimentally. Experimental research was carried out using optical methods like hot magnetophotoluminescence [57,59–61], quantum beat spectroscopy [62], hole burning [63], spin-flip Raman scattering [64], and reflectance difference spectroscopy [65,66]. Also, conductivity measurements in quasi-1D systems were employed to determine the $g$factors [67–69] of GaAs-based 2D hole gases. Hole systems studied over the years include 2D hole gases in both symmetric double heterostructures and inversion layers in single heterojunctions, with differerent dopants and crystallographic orientations. Despite extensive attention, there is no systematic general understanding of spin splitting for 2D holes, and no agreement regarding experimental values of spin splitting in various systems.

Most surprisingly, the situation is even more daring in the theoretical understanding of the $g$factor in hole systems. From a naive point of view, the coefficients of the Zeeman terms in the Luttinger Hamiltonian of Eq. (2), which directly couple angular momentum to magnetic field are often considered as defining the $g$factor [32,70]. Coupling of the magnetic field to the cube of angular momentum is weak, and such consideration leads to $g^* = 7.2$ for heavy holes defined by coupling of field to angular momentum. As we shall see, this definition of g^* is not related to any actual splitting of hole levels in two dimensions and is just one of the contributions to the Zeeman splitting of levels. The physics behind this story is that even if the constant κ were zero, due to the angular momentum-kinetic momentum interaction, orbital motion in a magnetic field leads to spin precession and Zeeman splitting on its own. This picture, for example, is the origin of the phenomenon of spin separation in magnetic focusing [12].

In order to achieve systematic understanding of the g factor in a 2D hole gas we will begin with the controversy of a definition of the g factor for 3D holes and in electronic systems with spin-orbit interactions. We first remark that our concern here is the band structure value of spin splitting of single-particle states. It is this value that is an important starting point for the consideration of many-body effects, such as, e.g., skyrmion spin textures. However, we will not treat many-body effects, such as exchange enhancement of g factor [71] in the present paper. The single-particle value for the g factor is clearly defined in systems without spin-orbit interactions, where it is indeed determined by the constant of direct coupling of the magnetic field to the spin operator. In systems with spin-orbit interactions, including hole systems, several of the proposed theories of the g factor attempt to take into account the idea that the orbital motion of carriers in the presence of magnetic field results in spin splitting of band states due to the coupling of orbital degrees of freedom to spin. For 3D holes, nearly 50 years ago, Bir and Pikus [43] proposed the following solution to the g factor problem. They used the same separation of the 3D hole Hamiltonian into symmetric and antisymmetric parts that we use here for 2D holes. The levels defined by the symmetric part E_n are Kramers degenerate. For large n, the asymmetric part of the Hamiltonian is treated as a perturbation splitting the doubly degenerate level E_n into two spin sublevels $E_{n,+}$ and $E_{n,-}$, so that $g = (E_{n,+} - E_{n,-})/\mu B$. The resulting Bir-Pikus g factor is defined by both the orbital constants defining hole mass, following the notion that spin-orbit coupling in the presence of a magnetic field causes the orbital motion to contribute to the g factor, and by constants of the direct coupling of the magnetic field to the spin operator. Later, Perel [72] applied an alternative and completely different Keller-Rubinov method for the semiclassical quantization of matrix Hamiltonians [73,74] to the treatment of Luttinger holes and confirmed the results for the g factor by Pikus and Bir.

We are now going to demonstrate that the spin splitting found by Bir and Pikus and Perel, while defining the spectroscopic splitting of hole levels that can be measured in transitions induced by an ac electric field (so-called combined

TABLE I. Allowed cyclotron transitions for holes in an infinite rectangular well in a magnetic field $0.5 < B < 0.9$ T. The regions are those plotted in Fig. 10. ↑ indicates an increase in a transition intensity with B, while ↓ indicates its decrease. A transition with decreasing intensity vanishes when $[\nu]$ changes.

Region	$[\nu]$	Partially filled level	Highest level with opposite parity	Allowed cyclotron transitions
I	8	7 odd	3 even	7 odd → 8 odd ↓, 6 odd → 7 odd ↑, 3 even → 4 even
II	7	7 odd	2 even	7 odd → 8 odd ↓, 6 odd → 7 odd ↑, 2 even → 3 even
III	6	6 odd	2 even	6 odd → 7 odd ↓, 5 odd → 6 odd ↑, 2 even → 3 even
IV	5	2 even	6 odd	2 even → 3 even ↓, 1 even → 2 even ↑, 6 odd → 7 odd
V	5	6 odd	1 even	6 odd → 7 odd ↓, 5 odd → 6 odd ↑, 1 even → 2 even
VI	4	5 odd	1 even	5 odd → 6 odd ↓, 4 odd → 5 odd ↑, 1 even → 2 even

resonance [53]), is not a true spin splitting that is relevant to hole spin resonance induced by an ac magnetic field, conductance spectroscopy of spin levels, and quantum bits. In order to do this and to establish the definition of the true g factor, we first revisit an analysis of the problem of the g factor in a simple model, which is actually important on its own: the g factor for electrons subject to Rashba interactions.

A. What is g factor in the presence of spin-orbit interactions: electrons with Rashba coupling

2D electrons in the presence of Rashba SO coupling in a perpendicular magnetic field are described by the Hamiltonian [53,75]

$$H_{eR}=\frac{\hbar eB}{c}\begin{pmatrix}\frac{1}{m}\left(a^\dagger a+\frac{1}{2}\right)+\frac{g}{4m_0} & i\alpha_R\ell a^\dagger\\ -i\alpha_R\ell a & \frac{1}{m}\left(a^\dagger a+\frac{1}{2}\right)-\frac{g}{4m_0}\end{pmatrix}. \tag{42}$$

Its $n\geqslant 1$ eigenvalues are

$$E^n_{e,\pm}=\hbar\omega_c\left[n\pm\sqrt{\left(\frac{gm}{4m_0}+\frac{1}{2}\right)^2+\alpha_R^2\ell^2m^2n}\right] \tag{43}$$

and eigenfunctions are the following spinors mixing up and down states with two Landau indices n and $n-1$:

$$\psi^n_{e,+}=\sqrt{\frac{1}{2}+\frac{g/m_0+2/m}{2\sqrt{(g/m_0+2/m)^2+16\alpha_R^2\ell^2n}}}\begin{pmatrix}u_n\\ \frac{2i\alpha_R\ell}{g/m_0+2/m+\sqrt{(g/m_0+2/m)^2+16\alpha_R\ell^2n}}u_{n-1}\end{pmatrix} \tag{44}$$

$$\psi^n_{e,-}=\sqrt{\frac{1}{2}+\frac{g/m_0+2/m}{2\sqrt{(g/m_0+2/m)^2+16\alpha_R^2\ell^2n}}}\begin{pmatrix}\frac{-2i\alpha_R\ell}{g/m_0+2/m+\sqrt{(g/m_0+2/m)^2+16\alpha_R\ell^2n}}u_n\\ u_{n-1}\end{pmatrix}. \tag{45}$$

The $n=0$ case is special:

$$E_0=\frac{\hbar\omega_c}{2}+\frac{g\mu B}{2}, \tag{46}$$

$$\psi^0_e=\begin{pmatrix}u_0\\ 0\end{pmatrix}. \tag{47}$$

Note that we assume $g<0$. Now, according to the prescription for finding the g factor at large n in Refs. [43,72], we should assume that the g factor defines the spin splitting of states with the same n, $g=(E^n_- - E^n_+)\mu B$. It is worth noticing that an ac electric field leads to transitions between such levels. However, this is not a true g factor. To see this, it is instructive to consider the limit of vanishing Rashba coupling, $\alpha_R\to 0$, in which the above eigenvalues are $E^n_\pm=\hbar\omega_c(n\pm\frac{1}{2}\pm\frac{gm}{4m_0})$ corresponding to pure up and down spinors: $\psi^n_-=\binom{0}{u_{n-1}}$ and $\psi^n_+=\binom{u_n}{0}$. Now, three issues are obvious. First, when the Rashba constant is zero, the g factor must be given by a constant (g) and not by $g_{\rm sp}=(E^n_{e,+}-E^n_{e,-})/\mu B=m_0/m-g$. Second, the spatial dependence of the spinors $\psi^n_\pm$ is different for Landau indices different by one, and therefore these states are not time-reversed pairs. Third, as a consequence of the latter property, the matrix element for coupling with an ac magnetic field, which is in the leading order, say, defined by the Pauli matrix σ_x, simply vanishes and does not lead to electron spin resonance transitions. Clearly, the appropriate time reversed pairs at zero Rashba coupling are states with $E_0=E^0_+$ and E^1_-, E^1_+ and $E^2_-,\ldots,E^{(n)}_+$ and $E^{(n+1)}_-$, where $n\geqslant 0$ are integers, and then the corresponding g factor is, of course, $-g$. Turning Rashba coupling back on, we see that the states $E^{(n)}_+$ and $E^{(n+1)}_-$ are no longer exactly time reversed, and there are small components of the spinors with distinct spatial dependencies in addition to time-reversed components in the leading order. However, the amplitude of transitions caused by an ac magnetic field between such states is much stronger than the amplitude of spin resonance transitions between the states $E^{(n)}_\pm$ with the same n, even when the full structure of spinors is taken into account for the latter pair of states. Thus it is natural to associate the g factor with energy separation between $E^{(n)}_+$ and $E^{(n+1)}_-$. In the presence of Rashba coupling,

$$g(n)=\frac{2m_0}{m}-\sqrt{\left(\frac{g}{2}+\frac{m_0}{m}\right)^2+4\alpha_R^2\ell^2m_0^2n}+\sqrt{\left(\frac{g}{2}+\frac{m_0}{m}\right)^2+4\alpha_R^2\ell^2m_0^2(n+1)}. \tag{48}$$

Hence even for electrons, in the presence of spin-orbit interactions, spin splitting depends not only on g but also on orbital constants, such as the electron mass m and spin-orbit constant α_R, as well as on the Landau index n and on the magnitude of the magnetic field. We reiterate that the physical meaning of such a dependence is that in the presence of spin-orbit coupling, orbital motion in a magnetic field results in spin splitting, or, in classical terms, results in additional spin precession. In the limit of strong Rashba coupling, spin splitting is formally determined by orbital constants, $g^*=2(E^{n+1}_- - E^n_+)=2m_0/m-2\alpha_R\ell m_0(\sqrt{n+1}+\sqrt{n})$. In this case, for high n, the ordering of levels can change, and the g factor defined this way can change sign.

Finally, in this section, we would like to emphasize, that this case of Rashba spectrum is a perfect illustration of the necessity to exercise caution in considering spin-orbit interactions and the definitions of g factors and effective masses. Indeed, at large $\frac{gm}{4m_0}+\frac{1}{2}$, and sufficiently small n, expansion of the energy (43) can lead to a definition of spin-dependent effective mass and spin-dependent cyclotron frequency:

$$\omega_c^\pm=\omega_c\left(1\pm\frac{\alpha_R^2\ell^2m^2}{\frac{gm}{2m_0}+1}\right). \tag{49}$$

The resolution of this dilemma is simply that in this range of parameters, it is somewhat meaningless to separate spin and

cyclotron splitting. For the Luttinger spectra, we encounter a such story for low-lying states outside the semiclassical regime.

B. g factor of 2D Luttinger holes

Having understood the g factor in the case of simple spin-orbit interactions in the previous section, we now define the g factor of Luttinger holes. For low-lying hole levels, the distinction between cyclotron and spin splitting is not meaningful, so we address the semiclassical case $n \gg 1$. We have already defined doubly degenerate levels E_{np} with even and odd eigenfunctions with respect to reflection about the $z = 0$ plane, and their splitting due to H_a into two spin sublevels $E_{n,+}$ and $E_{n,-}$. In the leading approximation, at high n, the average value of J_z in these states is $\pm 3/2$ for heavy holes and $\pm 1/2$ for light holes. However, in much the same way as the case for electrons in the previous section, in the leading order, the spatial dependence of the corresponding, odd and even heavy-hole wave functions is not the same, as it should be for time-reversed states. This spatial dependence is described by oscillator functions with Landau indices n and $n-3$ for any given n; that is, $\psi_{n,+} \propto (u_n,0,0,0)$ and $\psi_{n,-} \propto (0,0,0,u_{n-3})$. Thus, even if the spin operator describing transitions in an ac magnetic field couples odd and even spinors in the spin sector, the overlap of even and odd wave functions in the leading order is zero, because oscillator functions with Landau indices n and $n-3$ are orthogonal: $\int dx^T (u_n,0,0,0) J_x^3 (0,0,0,u_{n-3}) = 0$. We reiterate here again that spectroscopic splitting between states $n,+$ and $n,-$ can manifest in other types of transitions, such as combined resonance in an ac electric field. However, the corresponding splitting will not show up in pure spin resonance, and it is not appropriate to call it a g factor. Furthermore, direct evaluation shows that the corresponding constant for heavy holes is giant, exceeding ~ 40. For this reason, such splitting would be very difficult to access in conductance spectroscopy in quantum point contacts in a 2D hole gas. Thus the true g factor cannot be found using the procedures proposed in Refs. [43,72].

To find the true g factor, we consider a splitting between the states shown in Fig. 7. In the leading approximation for states with heavy mass in the $z$direction, these are the time-reversed states $\psi^{n,+}$ and $\psi^{n+3,-}$. Indeed, their leading order spinor structure is as follows: $\psi_{n,+} \propto (u_n,0,0,0)$ and $\psi_{n+3,-} \propto (0,0,0,u_n)$, i.e., their spatial dependencies are identical. Therefore we define the $g$factor for holes with heavy mass in the $z$direction as

$$g_h^* = 2(E^{n,-} - E^{n-3,+}). \tag{50}$$

For light holes, in the leading approximation, the time-reversed pair states are $\psi^{n,-}$ and $\psi^{n-1,+}$. The $g$factor for holes with light mass in the $z$direction is given by

$$g_l^* = 2(E^{n,-} - E^{n-1,+}). \tag{51}$$

We remark that when a magnetic field is in-plane and affects only the spin [76] with no orbital effects, the time-reversed pair states are formed from degenerate levels, and the definition of the g factor is straightforward.

We now present analytical results for the g factor of the 2D Luttinger holes in [001] grown quantum wells. Of primary interest for experiment is the g factor for the set of states associated with the ground state of heavy holes in the z direction. We therefore present here analytic results for this case. It is generally possible to find analytical results for high-n z-direction light-hole levels. For GaAs, however, there are some subtleties involved associated with the small separation between excited z-direction heavy-hole series of levels and similar light-hole states. We therefore address these states, as well as all low-lying states for z-direction heavy and light holes numerically.

The magnitude of the g factor for z-direction heavy holes in the semiclassical approximation is found from Eq. (34) using the wave vectors from Eq. (39) and the limits of small w and large n, in much the same way as in the computation of the in-plane effective mass. After tedious, but straightforward calculations, the effective g factor for the ground series of states with heavy-hole mass in the z direction is given by

$$g^* = 6\kappa + \frac{27}{2} q_0 - \frac{3\gamma_3^2}{\gamma_2} + \frac{3\gamma_3^2 \sqrt{\gamma_1^2 - 4\gamma_2^2}}{\pi \gamma_2^2} \times \cot\left(\frac{\pi}{2} \sqrt{\frac{\gamma_1 - 2\gamma_2}{\gamma_1 + 2\gamma_2}} \right). \tag{52}$$

This is our central result for the g factor. The g factor has contributions from orbital constants, and terms due to the size quantization besides the purely Zeeman coupling constants κ and q. The size quantization terms are independent of the well width provided that condition $\lambda q_z, \lambda/w \gg 1$ holds, in much the same way as for the effective masses defined by Eq. (41). Choosing the values of the Luttinger parameters for GaAs $\gamma_1 = 6.8, \gamma_2 = 2.1, \gamma_3 = 2.9, \kappa = 1.2$, and $q_0 = 0.04$, we find the effective g factor to be $g = 4.05$.

The semiclassical expression for the energy of the lowest subband of z-direction heavy holes that combines the cyclotron contribution defined by Eq. (41), and the Zeeman energy Eq. (52) is

$$E^{n,p} = \frac{(\gamma_1 - 2\gamma_2)\pi^2}{4w^2} + \left[\gamma_1 + \gamma_2 - \frac{3\gamma_3^2}{\gamma_2} + \frac{3\gamma_3^2}{\pi^2 \gamma_2^2} \times \sqrt{\gamma_1^2 - 4\gamma_2^2} \cot\left(\frac{\pi}{2} \sqrt{\frac{\gamma_1 - 2\gamma_2}{\gamma_1 + 2\gamma_2}} \right) \right] \times (n - 4p + 1) - 2\left(\gamma_1 + \gamma_2 - 3\kappa - \frac{27}{4} q_0 \right) p \quad (p = \pm 1). \tag{53}$$

Numerical evaluation of the spin splitting for all states, including high Landau indices but small size quantization energies, and low lying states, is based on the same definition of the g factor as for the semiclassical range of parameters. We plot in Fig. 11 the effective Landé factor for a 250 and 100 Å and for hole densities of 2×10^{10} and 10^{11} cm^{-2}. It is clear that the g factor values for holes in the narrow well are closer to the semiclassical limit of Eq. (52) that corresponds to the black line than the one for the wider well. This is due to the fact that with an increase in w, the coupling between spin and orbital motion increases, making the system deviate more from the semiclassical regime. We notice also, that the deviation is larger for a bigger density of holes. This can be explained by the larger index n of the partially filled level, which makes

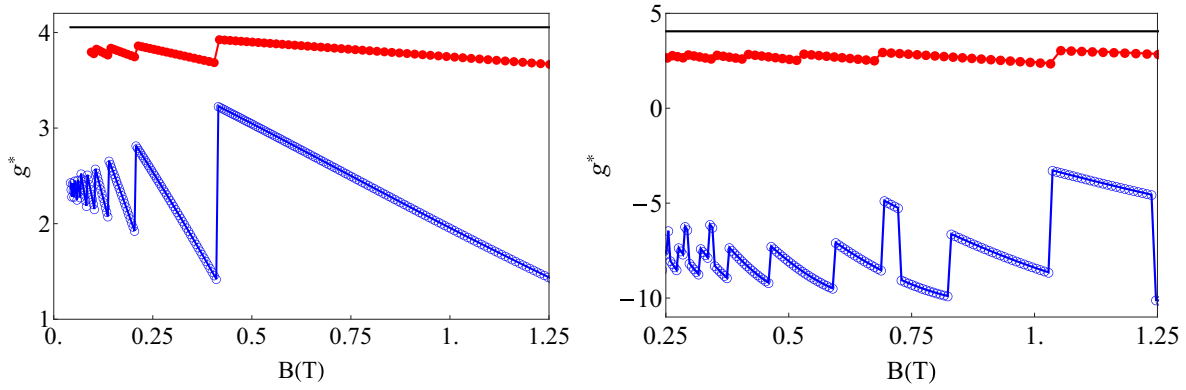

FIG. 11. (Color online) Effective Landé factor for crossing spectrum. The red lines (solid symbols) - well width of 100 Å, blue lines (open symbols) - well width of 250 Å. In the left panel the density is 2×10^{10} cm^{-2} and in the right panel the density is 10^{11} cm^{-2}.

$w^2 n$ larger, making analytical approximations that account for mixture of transverse and in-plane motion less viable.

Interpreting the spectra in terms of g factors is challenging because of the not fanlike, nonequidistant orbital spectra, which show numerous spectral crossings. The locations of the crossings depend on the potential profile of the quantum well in a given experimental setting.

Direct measurement of the effective Landé factor is achieved by spin magnetic resonance experiments with an oscillating in-plane magnetic field applied. The resonant peak appears at the frequency defined by the Zeeman energy. In the presence of an in-plane field $B_\parallel(\hat{x}\cos\omega t + \hat{y}\sin\omega t)$ the Hamiltonian is given by

$$H_\parallel = \frac{B_\parallel}{B}\left[\left(\kappa J_x + q_0 J_x^3\right)\cos\omega t + \left(\kappa J_y + q_0 J_y^3\right)\sin\omega t\right]. \quad (54)$$

Both the J_i and J_i^3 terms of this perturbation connect levels with index n to states with indices $n \pm 1$. The J_i^3 term also connects states with $n \pm 3$. As we discussed, the $g-$factor is meaningful only in the semiclassical limit, and we estimate the effect of such an in-plane field only for large n and a sufficiently narrow quantum well. For holes with heavy mass in the z direction, the $3/2$ component of the even wave function in this limit is much larger than the other three while for the odd state only the $-3/2$ component is relevant. As a consequence the ratio of the matrix elements of the in plane perturbation between n and $n-1$ and the matrix element between n and $n-3$ is given by

$$\left|\frac{\mathcal{V}_{n,n-1}}{\mathcal{V}_{n,n-3}}\right|^2 \approx \frac{\kappa^2\gamma_3^4\csc^4\left(\frac{\pi}{2}\sqrt{\frac{\gamma_1-2\gamma_2}{\gamma_1+2\gamma_2}}\right)}{4q_0^2 n^4\gamma_2^2(\gamma_2+\gamma_3)^2}\left[3-\cos\left(\pi\sqrt{\frac{\gamma_1-2\gamma_2}{\gamma_1+2\gamma_2}}\right)\right.$$
$$-\frac{2(\gamma_1-\gamma_2)}{\pi\gamma_2}\sqrt{\frac{\gamma_1-2\gamma_2}{\gamma_1+2\gamma_2}}$$
$$\left.\times\sin\left(\pi\sqrt{\frac{\gamma_1-2\gamma_2}{\gamma_1+2\gamma_2}}\right)\right]^2 \approx \frac{0.52}{n^4}. \quad (55)$$

We observe that the J_x^3 term leads to a much stronger transition than the J_x term. The spin resonance for the ground hole series of levels will determine the actual spacing between n odd and $n-3$ even, the "time-reversed" pair states in agreement with our definition of the g factor. We note that if the experiment involves series of levels with light-hole mass in the z direction, then spin resonance transitions connect the "time-reversed pair" states (n odd and $n-1$ even).

VII. ROLE OF ANISOTROPIC TERMS AND ADDITIONAL SPIN-ORBIT INTERACTIONS

A. Dresselhaus spin-orbit interaction

Besides the Luttinger Hamiltonian angular-momentum and momentum interactions described by Eq. (1), symmetry allows additional spin-orbit interactions associated with the lack of inversion symmetry or the asymmetry of the potential confining holes to two dimensions. Most notable are the Dresselhaus terms [77] due to the lack of inversion symmetry. These terms are most relevant to the case of double heterostructures with symmetric confinement, in which asymmetry induced by one-sided doping or external gate, and the corresponding Rashba-like terms are rather weak. For electrons, the Rashba and Dresselhaus terms are important for avoided crossings of the Landau levels belonging to a different size quantization subbands [78]. In a simplified treatment of 2D holes, it has been found that these low symmetry spin-orbit terms are capable of inducing spectral crossings and anticrossings in a magnetic field hole spectra in quantum dots [18]. As we have seen, such crossings, however, already arise due to the Luttinger interactions of Eq. (1). The question then is, what is the combined effect of all of these spin-orbit terms, and how, e.g., Dresselhaus interactions affect the Luttinger spectra of holes in a magnetic field.

Dresselhaus terms for holes at zero magnetic field have been discussed in Refs. [42,79]. It is convenient to write down the Hamiltonian describing these terms as

$$H_D = \gamma_v \mathbf{J}\cdot\kappa + \delta\gamma_v\left[\frac{13}{8}\mathbf{J}\cdot\kappa - \frac{1}{2}\sum_i J_i^3\kappa_i\right.$$
$$\left. - \frac{1}{2}\sum_i V_i\{k_i,(k^2-k_i^2/3)\}\right], \quad (56)$$

where

$$V_z = \left\{J_z, J_x^2 - J_y^2\right\}, \quad (57)$$

$$\kappa_z = \left\{k_z, k_x^2 - k_y^2\right\}, \quad (58)$$

and $V_{x(y)}$, and $\kappa_{x(y)}$ are defined using cyclic permutations of indices. The Dresselhaus constants for GaAs are $\gamma_v = -39$ eV Å^3 and $\delta\gamma_v = -35$ eV Å^3. In the presence of magnetic field, k_x and k_y are replaced with their operator expressions (4).

The symmetry of Dresselhaus interactions for holes is richer than that for electrons. Coupling for bulk electrons includes only terms containing κ_i, and such terms do not lead to linear in k coupling for z-direction heavy holes in [001] grown quantum wells. However, other Dresselhaus terms for bulk holes, such as, e.g., the V_i term gives rise to linear coupling in momentum for z-direction heavy holes [42].

In a magnetic field, Dresselhaus terms mix states with opposite parity and level indices n that differ by 2, 4, and 6, introducing additional splitting between even and odd states. This is because of the structure of the spinors of the odd and even states, and due to the linear and cubic in the wave vector contributions to the Dresselhaus spin-orbit coupling for holes in 2D, which couple oscillator functions with indices differing by one and three, correspondingly. Some of the crossings exhibited by the spectra of Luttinger holes described by Eq. (1) are transformed into anticrossings by Dresselhaus coupling, if the Dresselhaus interaction matrix element between states that cross is nonzero. In this case, the Dresselhaus interaction lifts the degeneracy. The Dresselhaus terms have a similar effect in electronic systems or in the simplified picture of hole spectra [80]. However, some of the crossings of Luttinger holes, most notably the crossing in the ground hole state, are not related to and remain unaffected by Dresselhaus interactions. The nonzero matrix elements of the Dresselhaus Hamiltonian (56) between states of an infinite rectangular quantum well [Eq. (17)] are presented in Appendix C.

Considering the role of Dresselhaus interactions in Eq. (56) that contain the operator k_z^3, a nontrivial problem arises in regularization. Recent work [81] suggests that the difficulties posed by this problem are unsurmountable and develops a scheme within the frame of a 14-band model in order to avoid this problem. We resolve this problem directly, and present our solution in Appendix B. Numerical results of the hole spectra in the presence of Dresselhaus terms are shown below. These results also take into account the effect of the nonaxial terms of Eq. (8).

B. Nonaxial terms

The last term of Eq. (8) has not yet been included in our analytical consideration. However, to a significant extent, the effects of anisotropy are included in our analytical consideration. In particular, most important are terms coupling z direction and in-plane motion, which are defined by the Luttinger constant γ_3 in our analytical approach. What is treated approximately in our analytical consideration is the effect of admixture of z-direction heavy-hole states with angular momentum projection $3/2$ $(-3/2)$ with z-direction light holes with angular momentum projection $-1/2$ $(1/2)$, for which only the part proportional to the combination of the Luttinger constants $\gamma_2 + \gamma_3$ is included. The remaining term proportional to $\gamma_2 - \gamma_3$, is not expected to result in any dramatic effect, and it is reasonable to treat this term as a perturbation for degenerate levels. The corresponding Hamiltonian is

$$H_N = -\frac{\gamma_2 - \gamma_3}{4}[(\hat{a}^\dagger)^2 J_-^2 + \hat{a}^2 J_+^2], \tag{59}$$

and its nonzero matrix elements between the states of an infinite rectangular quantum well with the same parity and Landau indices differing by 4 are given in Appendix D. This is a result of the structure of the spinors making matrix elements nonzero if $3/2$ and $-1/2$ components of the initial and final spinors (or their $-3/2$ and $1/2$ components) are characterized by oscillator functions with indices differing by two. For GaAs, numerical results demonstrate that the effect of $\gamma_2 - \gamma_3$ term is sufficiently small indeed, at least in the range of sufficiently small magnetic fields of interest here.

C. Energy spectra of holes in the presence of Dresselhaus and nonaxial terms

The results for the lowest five in-plane levels of the z-direction ground-state heavy holes series are presented in Fig. 12 for 250 Å (left) and 100 Å (right). We observe that the effects of the Dresselhaus and nonaxial terms are small at small magnetic fields and increase with the field.

As seen in the left panel of Fig. 13, the effects of the Dresselhaus and nonaxial terms are important for the second z-direction heavy-hole states for small Landau indices. This is due to the effective mass being negative [Eq. (41)] and levels

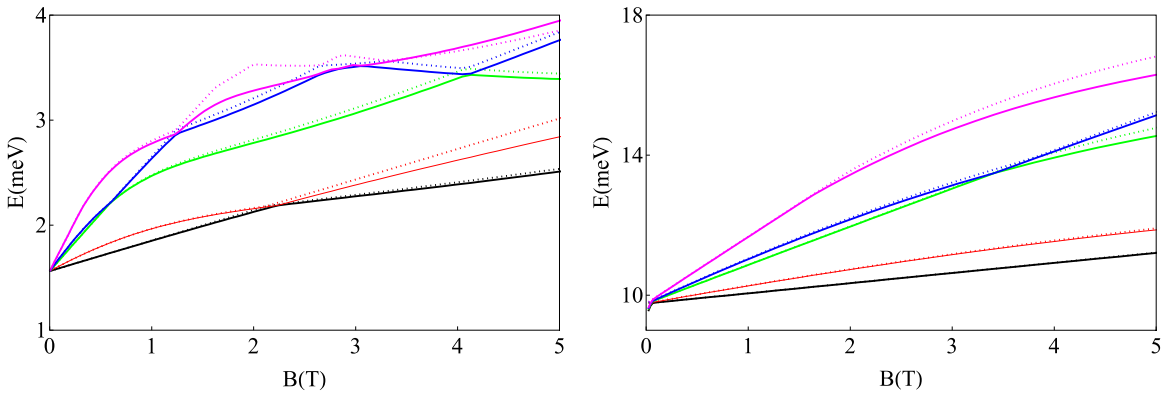

FIG. 12. (Color online) The spectra of holes in the presence of the Dresselhaus SO interaction and nonaxial terms (solid lines) compared to spectra obtained in their absence (dotted lines). The lowest five Landau levels of the lowest z-direction heavy hole state are plotted for a well width of 250 Å (left) and 100 Å (right).

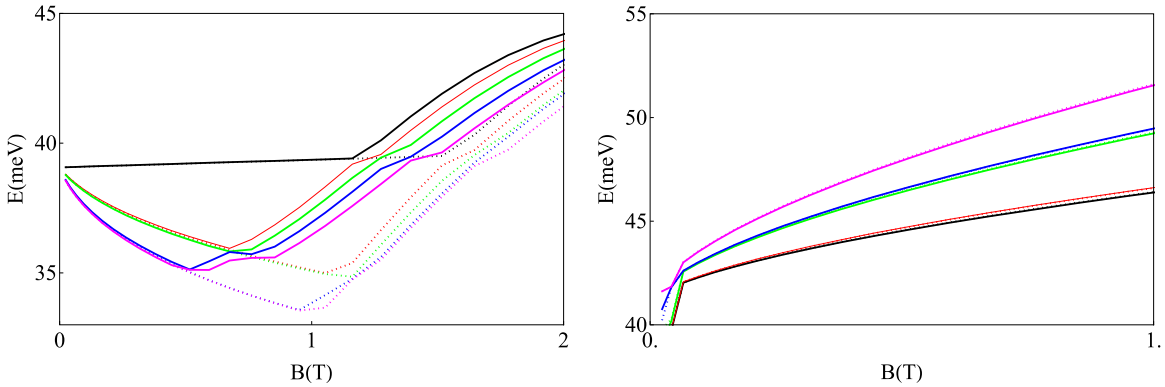

FIG. 13. (Color online) The spectra of holes in the presence of the Dresselhaus SO interaction and nonaxial term (solid line) compared to spectra obtained in their absence (dotted line) for the second z-direction heavy-hole state (left) and the first z-direction light-hole state (right) for 100-Å quantum well.

filling in reverse order. The effects on the z-direction light-hole state is small for small magnetic field as seen in the right panel of Fig. 13.

The hole spectrum at intermediate magnetic fields is presented in Fig. 14. We observe the there are numerous crossings and anticrossings. Some of the degeneracies leading to crossings have been lifted by the Dresselhaus and axial terms, but many crossings remain.

D. Effective mass and Landè factor in the presence of Dresselhaus and nonaxial term

To understand the problem, we focus our attention on a region near the crossings. After Dresselhaus terms and nonaxial effects are considered, the wave function becomes a linear combination of Landau level states $\sum_n c_n(u_n,u_{n-1},u_{n-2},u_{n-3})$. If only one coefficient c is significant, it is clear that the cyclotron resonance will not differ much from the case without perturbation. However, due to the numerous crossings in the spectra and relatively small separation between levels, wave functions have more than one sizable coefficient c. As an example, $\psi = -0.66|9,\text{odd}\rangle + 0.35|9,\text{even}\rangle + 0.64|5,\text{even}\rangle$, near the crossing of 9odd and 5even (coupled by Dresselhaus interactions). The 9-even state comes into play due to the nonaxial term coupling it to the 5-even state. From this level $|9,\text{odd}\rangle$, $|9,\text{even}\rangle$, and $|5,\text{even}\rangle$ would show cyclotron transition lines to all states containing $|10,\text{odd}\rangle$, $|10,\text{even}\rangle$, $|6,\text{even}\rangle$, $|8,\text{odd}\rangle$, $|8,\text{even}\rangle$, and $|4,\text{even}\rangle$. There are many such levels separated by differing energies. Therefore the measured cyclotron mass is a weighted average of all transition frequencies, which has little physical significance for any stand-alone pair of levels. The same story takes place in the spin resonance and measurement of g factors. Results for cyclotron mass and $g$factors, in the regions that are not strongly influenced by the level crossings are shown in Figs. 15 and 16.

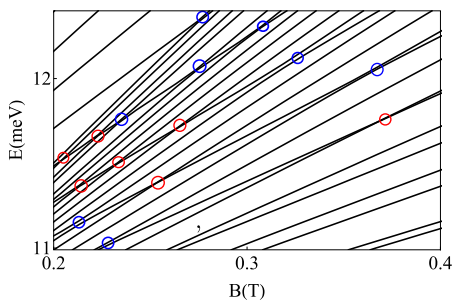

FIG. 14. (Color online) The energy spectra in the presence of the Dresselhaus and nonaxial terms show numerous crossings (red circles) and anticrossing (blue circles). The width of the well is 100 Å.

As we have discussed above in Secs. V and VI, introducing notions of effective masses and $g$factors for nonequidistant levels, in the presence of spectral crossings and peculiar order of level filling is sometimes ambiguous, as orbital and spin motion are completely entangled, especially for low-lying levels. In the semiclassical range of parameters, these problems do not arise, and the Luttinger hole system resembles the electron gas. This region is limited to small magnetic field and large n. However, in this range, due to the Dresselhaus terms, there are spin-orbit effects that are similar to the

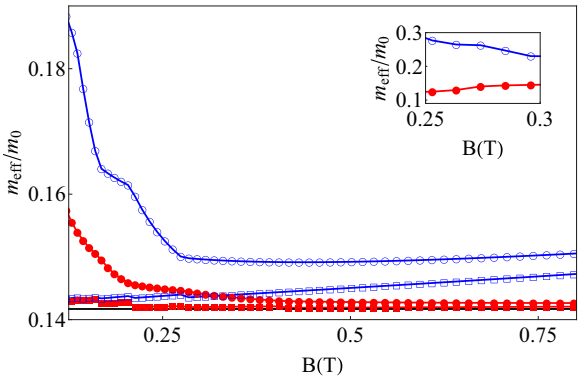

FIG. 15. (Color online) The cyclotron mass for the lowest band of the z-direction heavy holes in the presence of the Dresselhaus SO interaction and nonaxial terms. The hole density is 2×10^{10} cm^{-2}. The red lines (solid symbols) represent the cyclotron masses corresponding to even states while the blue lines (empty symbols) represent the ones corresponding to odd states. Circles represent the cyclotron mass in the presence of the Dresselhaus and nonaxial terms while squares represent cyclotron mass in their absence. The black line represents the semiclassical limit. (Inset) Cyclotron masses for these states at hole density 10^{11} cm^{-2}.

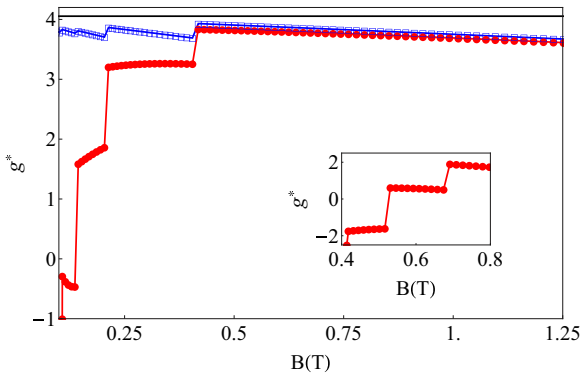

FIG. 16. (Color online) The effective Landé factor for the lowest band of the z-direction heavy holes in the presence of the Dresselhaus and nonaxial terms (red line - solid symbols) and without them (blue lines - empty symbols). The hole density is 2×10^{10} and the well width is 100 Å. The black line represents the semiclassical limit. (Inset) g factor for a 100-Å well with 10^{11} cm^{-2} holes, effect of the Dresselhaus and nonaxial terms included.

effects of Dresselhaus or Rashba terms for electrons in the semiclassical range, Sec. VI A. Analyzing experimental data in this range of parameters can provide information about Dresselhaus and similar effects for holes. For low-lying levels and states outside the semiclassical range, the effects of the Rashba and Dresselhaus terms are tangled with the Luttinger spin-orbit effects. The way to attempt to separate the role of various terms for such states could only be based on symmetry considerations, because Dresselhaus and Rashba terms, nonaxial terms, and principal Luttinger terms couple different states and result in different crossing/anticrossing effects because of their different symmetry.

VIII. SHUBNIKOV-DE HAAS OSCILLATIONS

In electronic systems, Shubnikov-de Haas oscillations, which are oscillations of the longitudinal conductivity σ_{xx} as the classically strong perpendicular magnetic field B_z is varied, have been extensively used in investigating the density of states of semiconductor structures, and peculiarities of electron spectra, such as the splitting of valley spectra and spin-orbit subbands in the presence of Dresselhaus and Rashba interactions. Shubnikov-de Haas oscillations have also been observed in numerous experiments in 2D hole systems, and it is important to understand what kind of effects can manifest themselves in experimental data. For example, if Shubnikov-de Haas oscillations in a hole system exhibit a beating pattern, would this be a consequence of Dresselhaus or Rashba spin-orbit interactions? Here we show that even in the absence of these interactions, crossings (or anticrossings) in the spectra of the 2D Luttinger holes lead to such patterns.

We take into account only hole states belonging to the Landau series of the first size quantized level of holes whose mass in the z direction is the heavy-hole mass. For the calculation of conductivity in the presence of a magnetic field, we use the symmetric gauge $\mathbf{A} = (By/2, -Bx/2, 0)$, and the in-plane components of the wave function with oscillator index n is given by

$$u_{n,X} = \frac{1}{\sqrt{L}} \frac{1}{\sqrt{2^n n! \sqrt{\pi}}} e^{-\frac{(x-X)^2 + i(x-2X)y}{2}} H_n(x - X). \quad (60)$$

For simplicity, we will assume that mobility of holes is defined by their short-range interactions with impurities with density ρ randomly distributed in the quantum well. At $w \ll 1$, the probability of spin(parity)-flip scattering of holes is negligible, and we take the impurity scattering matrix element $v_{ss'}(\mathbf{r}) = V\delta(\mathbf{r} - \mathbf{r}_i)\delta_{ss'}$, where $\mathbf{r}_i$ is the position of the impurity and and s and s' are the 3/2-spin components. To calculate the conductivity, we will extend to hole systems the procedure for 2D electrons from [82], treating the impurity scattering perturbatively. The Dyson's equation for the hole Green function $G(E) = (E - H)^{-1}$ reads $G^{s,s_1}_{n,p}(E) = G^{(0)}_{n,p} + G^{(0)}_{n,p} \sum_{s'} \Sigma^{s,s'}_{n,p} G^{s',s_1}_{n,p}(E)$, where Σ is the self-energy and $G^{(0)}_{n,p} = (E - E_{n,p})^{-1}$ is the Green function in the absence of impurities, with p labeling the parity of state. In the self-consistent Born approximation the self-energy is given by

$$\Sigma^{s,s_1}_{n,p}(E) = \rho \sum_i \sum_{\substack{n',X',p' \\ s',s'_1}} \int d\mathbf{r}_i \int d\mathbf{r} \int d\mathbf{r}' \mathcal{Z}^{n,p*}_s(z) u^*_{n+s,X}(x,y) v_{ss'}(\mathbf{r} - \mathbf{r}_i) \mathcal{Z}^{n',p'*}_{s'}(z) u_{n'+s',X'}(x,y)$$

$$\times \mathcal{Z}^{n',p'*}_{s'_1}(z') u^*_{n'+s'_1,X'}(x',y') v_{s'_1 s_1}(\mathbf{r}' - \mathbf{r}'_i) \mathcal{Z}^{n,p}_{s_1}(z) u_{n+s_1,X}(x',y') G^{s',s'_1}_{n',p'}(E), \quad (61)$$

where $\mathcal{Z}^{n',p'*}_{s'}$ is defined by Eqs. (10) and (12). The Landau level broadening Υ_{np} is calculated using the above formula for energies close to $E_{n,p}$ as $\Sigma^{ss}_{n,p} = \frac{1}{4}\Upsilon_{N,p} G_{n,p}(E)$. The density of states is

$$D(E) = \frac{1}{2\pi} \sum_{n,p} \sqrt{1 - \left(\frac{E - E_{n,p}}{\Upsilon_{n,p}}\right)^2}. \quad (62)$$

For short-range scatterers, the relaxation time is related to the level broadening as $\tau_f = 2\hbar^2\omega_c/(\pi\Upsilon^2)$.

We calculate the conductivity by using the Kubo formula

$$\sigma_{xx} = \frac{-ie^2}{\pi L^2} \sum_{n,X} \langle \psi_{n,p} | X \Im m G(E) [X, H] \Im m G(E) | \psi_{n,p} \rangle. \quad (63)$$

A perturbative expansion using the self-consistent Born approximation gives

$$\sigma_{xx} = \frac{e^2}{\pi^2\hbar}\sum_{n,p}\int dE\left(-\frac{\partial f_F(T)}{\partial E}\right)\left(\frac{\Upsilon^{xx}_{n,p}}{\Upsilon_{n,p}}\right)^2\left[1-\left(\frac{E-E_{n.p}}{\Upsilon n,p}\right)^2\right], \tag{64}$$

where T is the temperature, f_F is the Fermi function and

$$\left(\Upsilon^{xx}_{n,p}\right)^2 = \rho\sum_{s,s_1,s\prime,s_1\prime}\sum_{i}\sum_{n'X'p'}\int d\mathbf{r}_i\int d\mathbf{r}\int d\mathbf{r}'\mathcal{Z}^{n,p*}_{s}(z)u^*_{n+s,X}(x,y)\partial_y v_{ss'}(\mathbf{r}-\mathbf{r}_i)\mathcal{Z}^{n',p'*}_{s'}(z)u_{n'+s',X'}(x,y)$$
$$\times\,\mathcal{Z}^{n',p'*}_{s_1'}(z')u^*_{n'+s_{1'},X'}(x',y')\partial_{y'}v_{s_{1'}s_1}(\mathbf{r}'-\mathbf{r}'_i)\mathcal{Z}^{n,p}_{s_1}(z)u_{n+s_1,X}(x',y'). \tag{65}$$

The resulting pattern of oscillations of the longitudinal conductivity calculated taking into account Landau states belonging to the ground level of size quantization of z-direction heavy holes, in the absence of the Dresselhaus coupling and axial terms, is presented in Fig. 17. The system does exhibit some peculiar features originating from crossings in the hole spectra. However, the pattern is extremely complex, and the multiple conductivity maxima are too close to be separated. We note that the pattern of oscillations is qualitatively similar to those observed experimentally, e.g., in Ref. [58]. However, detailed comparison with experimental data is not feasible at this stage. Coulomb interactions of charge carriers that undoubtedly affect experiment are not taken into consideration by our procedure. A simple account of Hartree terms would not be sufficient, because exchange interactions are supposed to result in exchange enhancement of the Zeemann splitting, and in a much more complex way than for the electrons considered in Ref. [71]. However, the calculation presented here shows that the hole Shubnikov-de Haas patterns are characterized by beating-like structures even when spin-orbit interactions traditional for electron spectra, Rashba and Dresselhaus terms, are not taken into account, and only the Luttinnger Hamiltonian is included. Furthermore, complex patterns arise when only Landau states belonging to the ground level of size quantization of heavy holes are taken into account, but not the light-hole or excited heavy-hole Landau series. This picture is a direct consequence of nonequidistant, crossing levels.

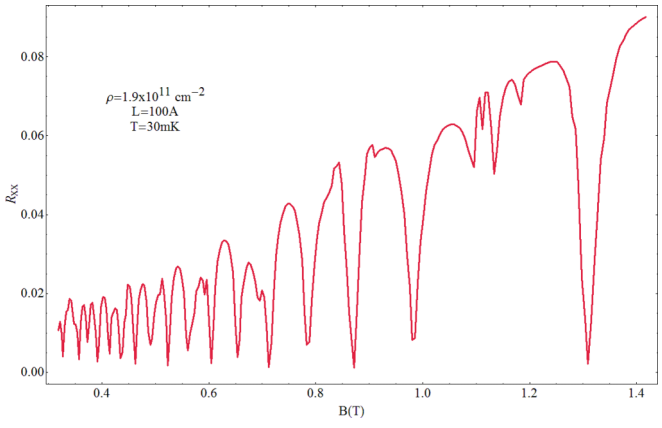

FIG. 17. (Color online) Shubnikov-de Haas oscillations of holes in an ideal quantum well without Dresselhaus-like perturbations. Features related to level crossings are obvious.

IX. CONCLUSIONS

We use the Luttinger Hamiltonian to describe the holes confined in GaAs quantum wells in the presence of a perpendicular magnetic field. We have identified the semiclassical regime, in which the physics of holes is reminiscent of the physics of electrons. We derive hole energies, and thereby the cyclotron masses and the g factors in the semiclassical regime analytically, by developing an analytical method of solving for size-quantized Luttinger holes in a perpendicular magnetic field. In the semiclassical regime with large Landau level indices, and for the size quantization energy much bigger than the cyclotron energy, the cyclotron mass coincides with the in-plane effective mass, calculated in the absence of a magnetic field. The g factor is defined not only by the constant of direct coupling κ of the angular momentum of holes with the magnetic field, but also by the Luttinger constants defining the effective masses of holes. For the 2D holes with heavy mass in [001] growth direction, in the semiclassical regime $g = 4.05$. This sheds light on why the g factor of holes measured [68] in a quantum point contact embedded in the 2D hole gas is $g^* = 5$, close to the 2D value, and is far from $6\kappa = 7.2$. In order to ensure the proper definition of the g factors of the holes, we used a solution of a simpler but illuminating problem of the electron g factor in the presence of spin-orbit Rashba interactions for illustration.

Outside the semiclassical range of parameters, holes behave as a species completely different from electrons. This is a consequence of the extraordinary strong angular momentum to momentum interactions, coupling of transverse and in-plane motion, mutual transformation of heavy and light holes with projections of angular momenta differing by ± 1, and coupling of heavy and light holes with angular momentum projections differing by ± 2. Spectra emerging for size- and magnetic-field-quantized holes are nonequidistant, not fanlike, and exhibit multiple crossings, including crossing in the ground level. Cyclotron masses of the holes in this regime arise from a few cyclotron transitions between levels with close energy separations. We explain theoretically why experiments do not show jumps in the value of the cyclotron masses when the integer part of the hole filling factors in the magnetic field changes. The only possible abrupt change in the value of the cyclotron mass may result from level crossing. Experimental observation of such changes can be used to identify crossings. We evaluate g factors and intensities of hole spin resonance. The values of cyclotron masses and g factors outside the semiclassical regime cannot be treated as band parameters, or

used for modeling of nanostructures and topological objects based on 2D hole systems.

We calculate the effect of the Dresselhaus and nonaxial terms in the magnetic hole quantized spectra. Dresselhaus terms of different symmetries are taken into account, and a regularization procedure is developed for the k_z^3 Dresselhaus terms, requiring special treatment. The Dresselhaus and nonaxial terms transform some of the crossings in the Luttinger hole magnetic spectra into anticrossings, but several crossings, including ground state crossing, are unaffected. Dresselhaus terms substantially affect the cyclotron masses in the range of magnetic fields containing crossings and anticrossings.

Holes exhibit complex patterns of the Shubnikov-de Haas oscillations. Oscillations are characterized by beating-like structures even when spin-orbit interactions traditional for electron spectra, the Rashba and Dresselhaus terms, are not taken into account, and only the Luttinger interactions are included. This property is also a consequence of nonequidistant spectra and level crossing. Crossings of levels are of critical importance, especially since novel fractional quantum Hall states with even denominator can appear at the crossings. Control of the nonequidistant levels and crossing structure by magnetic field can be used to control the Landau level mixing in hole systems, and thereby control hole-hole interactions, which are the subject of on-going research.

ACKNOWLEDGMENT

This work was supported by the US Department of Energy, Office of Basic Energy Sciences, Division of Materials Sciences and Engineering under Award DE-SC0010544.

APPENDIX A: CALCULATION OF WAVE VECTORS DESCRIBING THE HOLE STANDING WAVES IN THE SEMICLASSICAL APPROXIMATION

We first expand the wave vector, e.g., for the z-direction heavy-hole state keeping the usual term characterizing the z-direction plane wave and terms independent of and linear in the width of the quantum well (parameter w):

$$q_h = \frac{p\pi}{2w} + u + w\delta + O(w^2). \tag{A1}$$

For the calculation of the cyclotron mass in the semiclassical approximation, it is sufficient to consider the time-reversal symmetric part of the Hamiltonian and the corresponding energies only. We expand the energy of z-direction heavy- and light-hole states given by Eq. (20) in terms of q_z and in terms of n, and obtain Eqs. (37) and (38). Using the identity $E^n_{0,h}(q_h) = E^n_{0,l}(q_l)$, we find the relationship between q_l and q_h:

$$\begin{aligned} q_l &= \sqrt{\frac{\gamma_1-2\gamma_2}{\gamma_1+2\gamma_2}q_h^2 + \frac{4\gamma_2^2-12\gamma_3^2}{\gamma_1\gamma_2+2\gamma_2^2}(n-1)} \\ &= \sqrt{\frac{\gamma_1-2\gamma_2}{\gamma_1+2\gamma_2}}\frac{p\pi}{2w} + u\sqrt{\frac{\gamma_1-2\gamma_2}{\gamma_1+2\gamma_2}} + \sqrt{\frac{\gamma_1-2\gamma_2}{\gamma_1+2\gamma_2}} \\ &\quad\times\left[\frac{1}{p\pi}\frac{4\gamma_2^2-12\gamma_3^2}{\gamma_1\gamma_2-2\gamma_2^2}(n-1)+\delta\right]w + O(w^2). \end{aligned} \tag{A2}$$

Expansions (A1) and (A2) are used to solve Eq. (24). This quadratic equation in τ has two solutions, which in the leading order in w are given by

$$\tau_1 = -\frac{6\gamma_3^2(n-1)}{p^2\pi^2\gamma_2^2}w^2 + O(w^3), \tag{A3}$$

$$\tau_2 = -\frac{p^2\pi^2\gamma_2^2}{6(n-1)\gamma_3^2}\frac{\gamma_1-2\gamma_2}{\gamma_1+2\gamma_2}\frac{1}{w^2} + O(w^0). \tag{A4}$$

The same expressions for q_h and q_l can be used in the definition of τ]Eq. (25)]. In the leading order, the corresponding terms are

$$\begin{aligned} \tau = &-\frac{1}{u}\sqrt{\frac{\gamma_1-2\gamma_2}{\gamma_1+2\gamma_2}}\cot\left(\frac{p\pi}{2}\sqrt{\frac{\gamma_1-2\gamma_2}{\gamma_1+2\gamma_2}}\right)\frac{1}{w} \\ &+ O(w^0), \quad p \text{ odd}, \end{aligned} \tag{A5}$$

$$\begin{aligned} \tau = &\,u\sqrt{\frac{\gamma_1-2\gamma_2}{\gamma_1+2\gamma_2}}\cot\left(\frac{p\pi}{2}\sqrt{\frac{\gamma_1-2\gamma_2}{\gamma_1+2\gamma_2}}\right)w \\ &+ O(w^2), \quad p \text{ even}. \end{aligned} \tag{A6}$$

Comparison with Eqs. (A3) and (A4), which do not include linear in w and linear in $1/w$ terms in the corresponding expansions, indicates that it must be $u = 0$ in (A1). Therefore using Eq. (A1) in the definition of τ gives the following expansions:

$$\begin{aligned} \tau = &-\frac{1}{\delta}\sqrt{\frac{\gamma_1-2\gamma_2}{\gamma_1+2\gamma_2}}\cot\left(\frac{p\pi}{2}\sqrt{\frac{\gamma_1-2\gamma_2}{\gamma_1+2\gamma_2}}\right)\frac{1}{w^2} \\ &+ O(w^0), \quad p \text{ odd}, \end{aligned} \tag{A7}$$

$$\begin{aligned} \tau = &\,\delta\sqrt{\frac{\gamma_1-2\gamma_2}{\gamma_1+2\gamma_2}}\cot\left(\frac{p\pi}{2}\sqrt{\frac{\gamma_1-2\gamma_2}{\gamma_1+2\gamma_2}}\right)w^2 \\ &+ O(w^4), \quad p \text{ even}. \end{aligned} \tag{A8}$$

Now, comparing (A7) and (A8) with (A3) and (A4), we notice that the first solution appears for even p and the second solution is for odd p. Then, solving for δ, we obtain

$$\begin{aligned} \delta = &\frac{6(-1)^{p+1}}{p^2\pi^2}\frac{\gamma_3^2}{\gamma_2^2}\sqrt{\frac{\gamma_1+2\gamma_2}{\gamma_1-2\gamma_2}} \\ &\times\left[\tan\left(\frac{p\pi}{2}\sqrt{\frac{\gamma_1-2\gamma_2}{\gamma_1+2\gamma_2}}\right)\right]^{(-1)^p}(n-1). \end{aligned} \tag{A9}$$

For z-direction light holes,

$$q_h = \sqrt{\frac{\gamma_1+2\gamma_2}{\gamma_1-2\gamma_2}q_l^2 + \frac{-4\gamma_2^2+12\gamma_3^2}{\gamma_1\gamma_2-2\gamma_2^2}(n-1)}, \tag{A10}$$

and the proof is identical to the one presented above, with the only difference that the quantity under the square root is the inverse of that for heavy holes.

APPENDIX B: MATRIX ELEMENTS OF THE k_z^3 OPERATOR IN QUANTUM WELLS: REGULARIZATION PROCEDURE

In order to investigate the role of all Dresselhaus-type terms in the hole spectra allowed by symmetry, we need to project the bulk Dresselhaus terms given by Eq. (56) to the manifold of the 2D hole states. This requires calculating the matrix elements of the k_z^3 operator in the quantum wells. The potential of an infinite rectangular quantum well exhibits discontinuities at the edges of the well. As a result, the third derivative of the wave function over the coordinate along the growth axis is not well-defined. Ignoring the discontinuities when calculating the matrix elements of the operator k_z^3 generates peculiar and physically meaningless results, and a rigorous regularization procedure is needed.

We base our considerations on the idea that close crystalline bands can be considered on their own, once the perturbative admixture of all other bands accounting for the appearance of all terms with important symmetries is taken into account. This must be done using the natural boundary conditions that the wave functions and fluxes are continuous at the boundaries for all states within a group of close states. The regularization we find here satisfies these boundary conditions.

1. Infinitely deep quantum well

Let us consider first the case of an ideal infinitely deep quantum well of width w. The wave functions are the symmetric $\Psi_p^s(z)=\sqrt{\frac{1}{w}}\cos\frac{(2p+1)\pi z}{2w}$ and antisymmetric $\Psi_q^a(z)=\sqrt{\frac{1}{w}}\sin\frac{q\pi z}{w}$ states (p and q are integers). We notice that $\langle\Psi_q^a(z)|k_z^3|\Psi_p^s(z)\rangle=-i\frac{(-1)^{q-p}\pi^2(2p+1)^3q}{w^3[4q^2-(2p+1)^2]}$ and $\langle\Psi_p^s(z)|k_z^3|\Psi_q^a(z)\rangle=i\frac{(-1)^{q-p}4\pi^2q^3(2p+1)}{w^3[4q^2-(2p+1)^2]}$. Hence the operator k_z^3 looks nonHermitian! The origin of this behavior is the discontinuity of the confining potential.

A potential defining an infinitely deep well is

$$V(z)=\begin{cases}V_0(z), & \text{if} \quad |z|\leqslant w\\ \infty. & \text{otherwise}\end{cases}. \tag{B1}$$

The eigenfunction of the Schrödinger equation for the motion in this potential corresponding to the energy E will be denoted by $\Psi_E(z)$. The boundary conditions require that $\Psi_E(z)$ vanishes at $z=\pm w$.

To remove the discontinuity at the boundaries, we will use a "smooth" potential, whose behavior is regular, so that it leads to wave functions resulting in the hermitian projected operator k_z^3. We then take the limit, in which a smooth potential becomes an infinitely deep potential. Our choice for a smooth potential is

$$V_\Omega(z)=\begin{cases}V_0(z), & \text{if } |z|\leqslant w,\\ \frac{1}{2}m\Omega^2(z-w)^2+V_0'(w)(z-w), & \text{if } z>w,\\ \frac{1}{2}m\Omega^2(z+w)^2+V_0'(-w)(z+w), & \text{if } z<-w.\end{cases} \tag{B2}$$

This potential is continuous and differentiable everywhere, assuring a well-defined third derivative of the wave function. In the limit $\Omega\to\infty$, this potential reproduces the infinite well potential of Eq. (B1). The eigenfunction of the Schrödinger equation in the presence of this potential corresponding to energy E^Ω will be denoted by $\Psi_{\Omega,E_\Omega}(z)$. We show that in the limit of large Ω, $\Psi_{\Omega,E_\Omega}(z)$ converges toward $\Psi_E(z)$. The original potential of an infinitely deep well and its regularized counterpart are presented in Fig. 18.

A general normalizable wave function in the presence of the smooth potential is

$$\Psi_{\Omega,E_\Omega}(z)=\begin{cases}\Psi_{\Omega,E_\Omega,0}(z), & \text{if} \quad |z|\leqslant w,\\ \alpha_{\Omega,E_\Omega}D_{-\frac{1}{2}+\frac{E_\Omega}{\Omega}+\frac{V_0'(w)}{m\Omega^3}}\left(\sqrt{2m\Omega}(z-w)+\sqrt{\frac{2}{m\Omega^3}}V_0'(w)\right), & \text{if} \quad z>w,\\ \beta_{\Omega,E_\Omega}D_{-\frac{1}{2}+\frac{E_\Omega}{\Omega}+\frac{V_0'(-w)}{m\Omega^3}}\left(-\sqrt{2m\Omega}(z+w)-\sqrt{\frac{2}{m\Omega^3}}V_0'(-w)\right), & \text{if} \quad z>w,\end{cases} \tag{B3}$$

where D is the parabolic cylinder function [83] and $\Psi_{\Omega,E_\Omega,0}(z)$ is the solution Schrödinger equation inside the well $-\frac{1}{2m}\frac{\partial^2\Psi_{\Omega,E_\Omega,0}(z)}{\partial z^2}+V_0(z)\Psi_{\Omega,E_\Omega,0}(z)=E^\Omega\Psi_{\Omega,E_\Omega,0}(z)$.

The coefficients α and β are determined by imposing the continuity boundary condition on the wave function at $z=\pm w$ as

$$\alpha_{\Omega,E_\Omega}=\frac{\Psi_{\Omega,E_\Omega,0}(w)}{D_{-\frac{1}{2}+\frac{E_\Omega}{\Omega}+\frac{V_0'(w)}{m\Omega^3}}\left(\sqrt{\frac{2}{m\Omega^3}}V_0'(w)\right)}, \tag{B4}$$

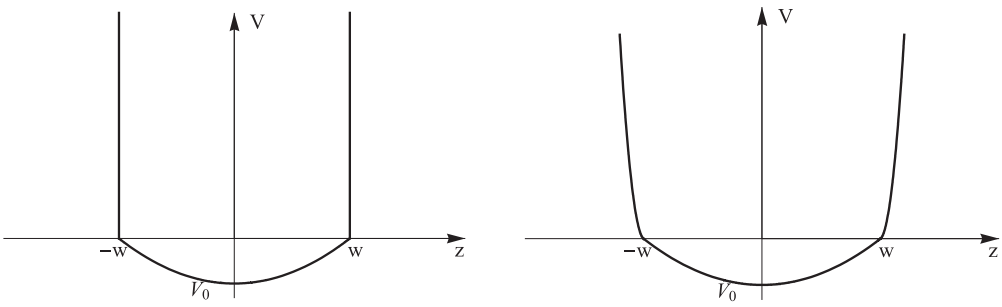

FIG. 18. Potential of an infinitely deep well (left) and its drivable counterpart (right).

$$\beta_{\Omega,E_\Omega}=\frac{\Psi_{\Omega,E_\Omega,0}(-w)}{D_{-\frac{1}{2}+\frac{E_\Omega}{\Omega}+\frac{V_0'(-w)}{m\Omega^3}}\left(-\sqrt{\frac{2}{m\Omega^3}}V_0'(-w)\right)}. \tag{B5}$$

Continuity of the derivative of the wave function at the boundaries of the quantum well requires that

$$\Psi'_{\Omega,E_\Omega,0}(w)=-\frac{\Psi_{\Omega,E_\Omega,0}(w)}{D_{-\frac{1}{2}+\frac{E_\Omega}{\Omega}+\frac{V_0'(w)}{m\Omega^3}}\left(\sqrt{\frac{2}{m\Omega^3}}V_0'(w)\right)}D_{\frac{1}{2}+\frac{E_\Omega}{\Omega}+\frac{V_0'(w)}{rm\Omega^3}}\left(\sqrt{\frac{2}{m\Omega^3}}V_0'(w)\right)\sqrt{2m\Omega}, \tag{B6}$$

$$\Psi'_{\Omega,E_\Omega,0}(-w)=\frac{\Psi_{\Omega,E_\Omega,0}(-w)}{D_{-\frac{1}{2}+\frac{E_\Omega}{\Omega}+\frac{V_0'(-w)}{m\Omega^3}}\left(-\sqrt{\frac{2}{m\Omega^3}}V_0'(-w)\right)}D_{\frac{1}{2}+\frac{E_\Omega}{\Omega}+\frac{V_0'(-w)}{m\Omega^3}}\left(-\sqrt{\frac{2}{m\Omega^3}}V_0'(-w)\right)\sqrt{2m\Omega}. \tag{B7}$$

Retaining only the leading terms in Ω, we find the relation between the wave function at $z=\pm w$ and its derivative:

$$\Psi'_{\Omega,E_\Omega,0}(w)=-\sqrt{m\Omega}\frac{2\Gamma\left(\frac{3}{4}\right)}{\Gamma\left(\frac{1}{4}\right)}\Psi_{\Omega,E_\Omega,0}(w)+O\left(\frac{1}{\sqrt{\Omega}}\right), \tag{B8}$$

$$\Psi'_{\Omega,E_\Omega,0}(-w)=\sqrt{m\Omega}\frac{2\Gamma\left(\frac{3}{4}\right)}{\Gamma\left(\frac{1}{4}\right)}\Psi_{\Omega,E_\Omega,0}(-w)+O\left(\frac{1}{\sqrt{\Omega}}\right). \tag{B9}$$

We see that in the limit of $\Omega\to\infty$, the derivative $\Psi'_{\Omega,E_\Omega,0}(w)$ cannot be infinite as it is expressed using only parabolic cylinder functions, which do not have poles. This requires that $\Psi_{\Omega,E_\Omega,0}(\pm w)\to 0$, which represents the boundary conditions imposed on the original discontinuous potential, and thus, $\Psi_{\Omega,E_\Omega,0}\to\Psi_E$.

The integral describing the matrix element of k_z^3 between the states characterized by wave functions Ψ_{Ω,E_Ω^2} and Ψ_{Ω,E_Ω^1} of the smooth potential can be split in three parts $\int_{-\infty}^{\infty}\Psi^*_{\Omega,E_\Omega^2}(z)\frac{\partial^3\Psi_{\Omega,E_\Omega^1}(z)}{\partial z^3}dz=\int_{-w}^{w}\ldots+\int_{w}^{\infty}\ldots+\int_{-\infty}^{-w}\ldots=I_1+I_2+I_3$. The first integral converges in the large Ω limit to the value calculated using the discontinuous potential $\int_w^w\Psi^*_{E_2}(z)\frac{\partial^3\Psi_{E_1}(z)}{\partial z^3}dz$.

Evaluation of the quadratures outside the well is simplified using the transformation of variables

$$I_2=2m\Omega\alpha^*_{\Omega,E_\Omega^2}\alpha_{\Omega,E_\Omega^1}\int_{\sqrt{\frac{2}{m\Omega^3}}V_0'(w)}^{\infty}D_{-\frac{1}{2}+\frac{E_\Omega^2}{\Omega}+\frac{V_0'(w)}{m\Omega^3}}(\xi)\frac{\partial^3}{\partial\xi^3}D_{-\frac{1}{2}+\frac{E_\Omega^1}{\Omega}+\frac{V_0'(w)}{m\Omega^3}}(\xi)d\xi, \tag{B10}$$

$$I_3=-2m\Omega\beta^*_{\Omega,E_\Omega^2}\beta_{\Omega,E_\Omega^1}\int_{\sqrt{\frac{2}{m\Omega^3}}V_0'(-w)}^{\infty}D_{-\frac{1}{2}+\frac{E_\Omega^2}{\Omega}+\frac{V_0'(-w)}{m\Omega^3}}(\xi)\frac{\partial^3}{\partial\xi^3}D_{-\frac{1}{2}+\frac{E_\Omega^1}{\Omega}+\frac{V_0'(-w)}{m\Omega^3}}(\xi)d\xi. \tag{B11}$$

Retaining only the leading order terms in Ω, we reduce the above quadratures to

$$I_2=2m\Omega\frac{\Psi^*_{\Omega,E_\Omega^2,0}(w)}{D_{-\frac{1}{2}}(0)}\frac{\Psi_{\Omega,E_\Omega^1,0}(w)}{D_{-\frac{1}{2}}(0)}\int_0^{\infty}D_{-\frac{1}{2}}(\xi)\frac{\partial^3}{\partial\xi^3}D_{-\frac{1}{2}}(\xi)d\xi, \tag{B12}$$

$$I_3=-2m\Omega\frac{\Psi^*_{\Omega,E_\Omega^2,0}(-w)}{D_{-\frac{1}{2}}(0)}\frac{\Psi_{\Omega,E_\Omega^1,0}(-w)}{D_{-\frac{1}{2}}(0)}\int_0^{\infty}D_{-\frac{1}{2}}(\xi)\frac{\partial^3}{\partial\xi^3}D_{-\frac{1}{2}}(\xi)d\xi. \tag{B13}$$

We use the following formula for the derivative of the parabolic cylinder functions [83]:

$$\frac{\partial^3D_\nu(t)}{\partial t^3}=\frac{1}{8}(\nu^2-3\nu+2)\nu D_{\nu-3}(t)-\frac{3}{8}\nu^2D_{\nu-1}(t)+\frac{1}{8}(3\nu+3)D_{\nu+1}(t)-D_{\nu+3}(t), \tag{B14}$$

and the expression for an integral of product of D's [83]

$$\int_0^{\infty}D_\alpha(t)D_\nu(t)\,dt=\frac{2^{\frac{1}{2}(-\alpha-\nu-3)}\left(\Gamma\left(-\frac{\alpha}{2}\right)\Gamma\left(\frac{1-\nu}{2}\right)-\Gamma\left(\frac{1-\alpha}{2}\right)\Gamma\left(-\frac{\nu}{2}\right)\right)}{(\alpha-\nu)\Gamma(-\alpha)\Gamma(-\nu)} \tag{B15}$$

in order to determine the value of quadrature that is present in Eqs. (B12) and (B13), which is

$$\int_0^{\infty}D_{-\frac{1}{2}}(\xi)\frac{\partial^3}{\partial\xi^3}D_{-\frac{1}{2}}(\xi)d\xi=\frac{\Gamma^2\left(\frac{3}{4}\right)}{2\pi\sqrt{2}}. \tag{B16}$$

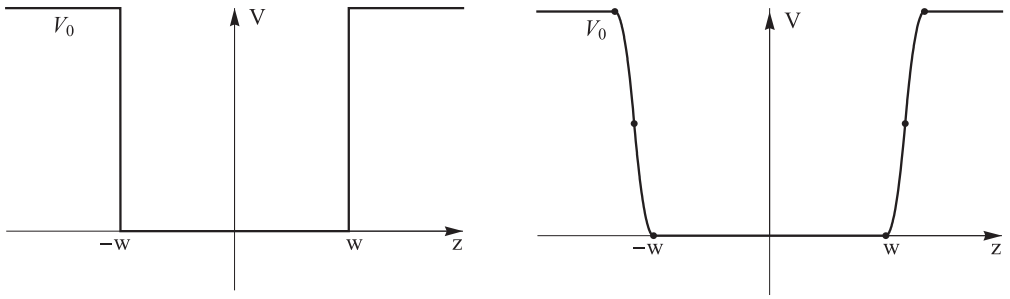

FIG. 19. Potential of a finite well (left) and its differentiable counterpart (right).

Using the result (B16), we obtain the expressions for integrals outside the quantum well:

$$I_2 = \frac{m\Omega}{2\pi^2}\Gamma^2\left(\frac{3}{4}\right)\Gamma^2\left(\frac{1}{4}\right)\Psi^*_{\Omega,E^2_\Omega,0}(w)\Psi_{\Omega,E^1_\Omega,0}(w) = m\Omega\Psi^*_{\Omega,E^2_\Omega,0}(w)\Psi_{\Omega,E^1_\Omega,0}(w), \tag{B17}$$

$$I_3 = -\frac{m\Omega}{2\pi^2}\Gamma^2\left(\frac{3}{4}\right)\Gamma^2\left(\frac{1}{4}\right)\Psi^*_{\Omega,E^2_\Omega,0}(-w)\Psi_{\Omega,E^1_\Omega,0}(-w) = -m\Omega\Psi^*_{\Omega,E^2_\Omega,0}(-w)\Psi_{\Omega,E^1_\Omega,0}(-w). \tag{B18}$$

Using the relation between values of the wave function and its derivative at the boundaries, Eqs. (B8) and (B9), we find that the contributions to the integral from z outside the well are

$$I_2 = \tfrac{1}{2}\Psi'^*_{\Omega,E^2_\Omega,0}(w)\Psi'_{\Omega,E^1_\Omega,0}(w), \tag{B19}$$

$$I_3 = -\tfrac{1}{2}\Psi'^*_{\Omega,E^2_\Omega,0}(-w)\Psi'_{\Omega,E^1_\Omega,0}(-w). \tag{B20}$$

Adding all parts together, we determine the value of the k_z^3 matrix element:

$$\left\langle\Psi_{E_2}\left|k_z^3\right|\Psi_{E_1}\right\rangle = i\int_{-w}^{w}\Psi^*_{E_2}(z)\frac{\partial^3\Psi_{E_1}(z)}{\partial z^3}dz + \frac{i}{2}\Psi'^*_{E_2}(w)\Psi'_{E_1}(w) - \frac{i}{2}\Psi'^*_{E_2}(-w)\Psi'_{E_1}(-w). \tag{B21}$$

2. Quantum well with finite depth

We now develop the regularization procedure for the k_z^3 averages in a well of finite depth. The potential is discontinuous at the boundaries, but the potential jump is finite. In general, the potential can be a smooth function, both inside and outside the well. From the previous consideration, we see that the regularization scheme is independent of the details of the potential. Hence we take the potential to be constant both inside and outside the well,

$$V(z) = \begin{cases} 0, & \text{if} \quad |z| \leqslant w \\ V_0, & \text{otherwise} \end{cases}. \tag{B22}$$

The wave function corresponding to energy E is denoted by Ψ_E.

The procedure is similar to that used for an infinitely deep quantum well. The potential is regularized using a parameter, that eventually will be taken to infinity. The matrix element is evaluated near the boundaries, and the limit for large potential parameter is considered. The smooth potential differs from the discontinuous one only in a small region near the boundaries of the quantum well:

$$V_\Omega(z) = \begin{cases} V_0, & \text{if} \quad z < -w - \frac{2}{\Omega}\sqrt{\frac{V_0}{m}}, \\ V_0 - \frac{1}{2}m\Omega^2\left(z + w + \frac{2}{\Omega}\sqrt{\frac{V_0}{m}}\right)^2, & \text{if} \quad -w - \frac{2}{\Omega}\sqrt{\frac{V_0}{m}} \leqslant z < -w - \frac{1}{\Omega}\sqrt{\frac{V_0}{m}}, \\ \frac{1}{2}m\Omega^2(z+w)^2, & \text{if} \quad -w - \frac{1}{\Omega}\sqrt{\frac{V_0}{m}} \leqslant z < -w, \\ 0, & \text{if} \quad |z| \leqslant w, \\ \frac{1}{2}m\Omega^2(z-w)^2, & \text{if} \quad w < z \leqslant w + \frac{1}{\Omega}\sqrt{\frac{V_0}{m}}, \\ V_0 - \frac{1}{2}m\Omega^2\left(z - w - \frac{2}{\Omega}\sqrt{\frac{V_0}{m}}\right)^2, & \text{if} \quad w + \frac{1}{\Omega}\sqrt{\frac{V_0}{m}} < z \leqslant w + \frac{2}{\Omega}\sqrt{\frac{V_0}{m}}, \\ V_0, & \text{if} \quad z > w + \frac{2}{\Omega}\sqrt{\frac{V_0}{m}}. \end{cases} \tag{B23}$$

It is continuous and differentiable everywhere. The original and modified potential are plotted in Fig. 19.

The eigenfunction corresponding to energy E_Ω is

$$\Psi_{\Omega,E_\Omega}(z)=\begin{cases}\Psi_{\Omega,E_\Omega,1,L}(z), & \text{if} \quad z<-w-\frac{2}{\Omega}\sqrt{\frac{V_0}{m}},\\ \gamma_{\Omega,E_\Omega,L}D_{-\frac{1}{2}-\frac{i(E_\Omega-V_0)}{2\Omega}}\left[e^{\frac{i\pi}{4}}\left(\sqrt{2m\Omega}(w+z)+\sqrt{\frac{8V_0}{\Omega}}\right)\right] & \\ +\delta_{\Omega,E_\Omega,L}D_{-\frac{1}{2}+\frac{i(E_\Omega-V_0)}{2\Omega}}\left[e^{\frac{3i\pi}{4}}\left(\sqrt{2m\Omega}(w+z)+\sqrt{\frac{8V_0}{\Omega}}\right)\right], & \text{if} \quad -w-\frac{2}{\Omega}\sqrt{\frac{V_0}{m}}\leqslant z<-w-\frac{1}{\Omega}\sqrt{\frac{V_0}{m}},\\ \alpha_{\Omega,E_\Omega,L}D_{-\frac{1}{2}+\frac{E_\Omega}{\hbar\Omega}}[\sqrt{2m\Omega}(w+z)] & \\ +\beta_{\Omega,E_\Omega,L}D_{-\frac{1}{2}+\frac{E_\Omega}{\hbar\Omega}}[-\sqrt{2m\Omega}(w+z)], & \text{if} \quad -w-\frac{1}{\Omega}\sqrt{\frac{V_0}{m}}\leqslant z<-w,\\ \Psi_{\Omega,E_\Omega,0}(z), & \text{if} \quad |z|\leqslant w,\\ \alpha_{\Omega,E_\Omega,R}D_{-\frac{1}{2}+\frac{E_\Omega}{\Omega}}[\sqrt{2m\Omega}(z-w)] & \\ +\beta_{\Omega,E_\Omega,R}D_{-\frac{1}{2}+\frac{E}{\Omega}}[-\sqrt{2m\Omega}(z-w)] & \text{if} \quad w<z\leqslant w+\frac{1}{\Omega}\sqrt{\frac{V_0}{m}},\\ \gamma_{\Omega,E_\Omega,R}D_{-\frac{1}{2}-\frac{i(E_\Omega-V_0)}{2\Omega}}\left[e^{\frac{i\pi}{4}}\left(\sqrt{2m\Omega}(z-w)+\sqrt{\frac{8V_0}{\Omega}}\right)\right] & \\ +\delta_{\Omega,E_\Omega,R}D_{-\frac{1}{2}+\frac{i(E_\Omega-V_0)}{2\Omega}}\left[e^{\frac{3i\pi}{4}}\left(\sqrt{2m\Omega}(z-w)+\sqrt{\frac{8V_0}{\Omega}}\right)\right], & \text{if} \quad w+\frac{1}{\Omega}\sqrt{\frac{V_0}{m}}<z\leqslant w+\frac{2}{\Omega}\sqrt{\frac{V_0}{m}},\\ \Psi_{\Omega,E_\Omega,1,R}(z), & \text{if} \quad z>w+\frac{2}{\Omega}\sqrt{\frac{V_0}{m}},\end{cases} \tag{B24}$$

where $\Psi_{\Omega,E_\Omega,0}$ and $\Psi_{\Omega,E_\Omega,1}$ represents the solutions of Schrödinger equation inside and outside the quantum well $-\frac{1}{2m}\frac{\partial^2\Psi_{\Omega,E_\Omega,0}(z)}{\partial z^2}=E_\Omega\Psi_{\Omega,E_\Omega,0}(z)$, $-\frac{1}{2m}\frac{\partial^2\Psi_{\Omega,E_\Omega,1}(z)}{\partial z^2}+V_0\Psi_{\Omega,E_\Omega,1}(z)=E_\Omega\Psi_{\Omega,E,1}(z)$, indices L and R refers to left ($z<-w$) and right ($z>w$) of the well.

Continuity conditions imposed on the wave functions and their derivative determine the coefficients α, β, γ and δ. Retaining only the leading terms in Ω, we find

$$\alpha_{\Omega,E_\Omega,L}=\beta_{\Omega,E_\Omega,L}=\frac{\Gamma\left(\frac{3}{4}\right)}{\sqrt{2\sqrt{2}\pi}}\Psi_{\Omega,E_\Omega,0}(-w), \tag{B25}$$

$$\gamma_{\Omega,E_\Omega,L}=\delta_{\Omega,E_\Omega,L}=\frac{\Gamma\left(\frac{3}{4}\right)}{\sqrt{2\sqrt{2}\pi}}\Psi_{\Omega,E_\Omega,1,L}(-w), \tag{B26}$$

$$\alpha_{\Omega,E_\Omega,R}=\beta_{\Omega,E_\Omega,R}=\frac{\Gamma\left(\frac{3}{4}\right)}{\sqrt{2\sqrt{2}\pi}}\Psi_{\Omega,E_\Omega,0}(w), \tag{B27}$$

$$\gamma_{\Omega,E_\Omega,R}=\delta_{\Omega,E_\Omega,R}=\frac{\Gamma\left(\frac{3}{4}\right)}{\sqrt{2\sqrt{2}\pi}}\Psi_{\Omega,E_\Omega,1,R}(w). \tag{B28}$$

The matrix element integral is given by the following terms: $\int_{-\infty}^{\infty}\Psi^*_{\Omega,E^2_\Omega}(z)\frac{\partial^3\Psi_{\Omega,E^1_\Omega}(z)}{\partial z^3}dz=\int_{-\infty}^{-w-\frac{2}{\Omega}\sqrt{\frac{V_0}{m}}}\ldots+\int_{-w-\frac{2}{\Omega}\sqrt{\frac{V_0}{m}}}^{-w-\frac{1}{\Omega}\sqrt{\frac{V_0}{m}}}\ldots+\int_{-w-\frac{1}{\Omega}\sqrt{\frac{V_0}{m}}}^{-w}\ldots+\int_{-w}^{w}\ldots+\int_{w}^{w+\frac{1}{\Omega}\sqrt{\frac{V_0}{m}}}\ldots+\int_{w+\frac{1}{\Omega}\sqrt{\frac{V_0}{m}}}^{w+\frac{2}{\Omega}\sqrt{\frac{V_0}{m}}}\ldots+\int_{w+\frac{2}{\Omega}\sqrt{\frac{V_0}{m}}}^{\infty}\ldots=I_1+I_2+I_3+I_4+I_5+I_6+I_7$. The integrals I_1, I_4 and I_5 converge to their respective values for the discontinuous potential.

Using the Taylor expansion of the parabolic cylinder functions [83]

$$D_\nu(t)\simeq\frac{2^{\nu/2}\sqrt{\pi}}{\Gamma\left(\frac{1-\nu}{2}\right)}-\frac{2^{\frac{\nu+1}{2}}\sqrt{\pi}t}{\Gamma\left(-\frac{\nu}{2}\right)}-\frac{2^{\frac{\nu}{2}-2}\sqrt{\pi}(2\nu+1)t^2}{\Gamma\left(\frac{1-\nu}{2}\right)}+\frac{2^{\frac{\nu-3}{2}}\sqrt{\pi}(2\nu+1)t^3}{3\Gamma\left(-\frac{\nu}{2}\right)}+\frac{2^{\frac{\nu}{2}-5}\sqrt{\pi}(4\nu^2+4\nu+3)t^4}{3\Gamma\left(\frac{1-\nu}{2}\right)}+O(t^5), \tag{B29}$$

we calculate integrals over connecting regions. In the leading order in Ω, these are

$$\begin{aligned}I_2&\simeq\frac{\Gamma^2\left(\frac{3}{4}\right)m\Omega}{\sqrt{2}\pi}\Psi^*_{\Omega,E^2_\Omega,1,R}(-w)\Psi_{\Omega,E^1_\Omega,1,R}(-w)\int_{-2\sqrt{\frac{2V_0}{\Omega}}}^{-\sqrt{\frac{2V_0}{\Omega}}}\left[D_{-\frac{1}{2}}\left(e^{-\frac{i\pi}{4}}\xi\right)+D_{-\frac{1}{2}}\left(e^{-\frac{3i\pi}{4}}\xi\right)\right]\frac{\partial^3}{\partial\xi^3}\left[D_{-\frac{1}{2}}\left(e^{\frac{i\pi}{4}}\xi\right)+D_{-\frac{1}{2}}\left(e^{\frac{3i\pi}{4}}\xi\right)\right]d\xi\\ &\simeq-\frac{3mV_0}{4}\Psi^*_{\Omega,E^2_\Omega,1,R}(-w)\Psi_{\Omega,E^1_\Omega,1,R}(-w),\end{aligned} \tag{B30}$$

$$\begin{aligned}I_3&\simeq\frac{\Gamma^2\left(\frac{3}{4}\right)m\Omega}{\sqrt{2}\pi}\Psi^*_{\Omega,E^2_\Omega,0}(-w)\Psi_{\Omega,E^1_\Omega,0}(-w)\int_{-\sqrt{\frac{2V_0}{\Omega}}}^{0}[D_{-\frac{1}{2}}(\xi)+D_{-\frac{1}{2}}(\xi)]\frac{\partial^3}{\partial\xi^3}[D_{-\frac{1}{2}}(\xi)+D_{-\frac{1}{2}}(\xi)]d\xi\\ &\simeq-\frac{mV_0}{4}\Psi^*_{\Omega,E^2_\Omega,0}(-w)\Psi_{\Omega,E^1_\Omega,0}(-w),\end{aligned} \tag{B31}$$

$$I_5 \simeq \frac{\Gamma^2\left(\frac{3}{4}\right)m\Omega}{\sqrt{2}\pi}\Psi^*_{\Omega,E^2_\Omega,1,R}(w)\Psi_{\Omega,E^1_\Omega,1,R}(w)\int_{\sqrt{\frac{2V_0}{\Omega}}}^{2\sqrt{\frac{2V_0}{\Omega}}}\left[D_{-\frac{1}{2}}\left(e^{-\frac{i\pi}{4}}\xi\right)+D_{-\frac{1}{2}}\left(e^{-\frac{3i\pi}{4}}\xi\right)\right]\frac{\partial^3}{\partial\xi^3}\left[D_{-\frac{1}{2}}\left(e^{\frac{i\pi}{4}}\xi\right)+D_{-\frac{1}{2}}\left(e^{\frac{3i\pi}{4}}\xi\right)\right]d\xi$$
$$\simeq \frac{3mV_0}{4}\Psi^*_{\Omega,E^2_\Omega,1,R}(w)\Psi_{\Omega,E^1_\Omega,1,R}, \tag{B32}$$

$$I_6 \simeq \frac{\Gamma^2\left(\frac{3}{4}\right)m\Omega}{\sqrt{2}\pi}\Psi^*_{\Omega,E^2_\Omega,0}(w)\Psi_{\Omega,E^1_\Omega,0}(w)\int_{-\sqrt{\frac{2V_0}{\Omega}}}^{0}[D_{-\frac{1}{2}}(\xi)+D_{-\frac{1}{2}}(\xi)]\frac{\partial^3}{\partial\xi^3}[D_{-\frac{1}{2}}(\xi)+D_{-\frac{1}{2}}(\xi)]d\xi$$
$$\simeq \frac{mV_0}{4}\Psi^*_{\Omega,E^2_\Omega,0}(w)\Psi_{\Omega,E^1_\Omega,0}(w). \tag{B33}$$

The regularization procedure now reads

$$\langle\Psi_{E_2}|k_z^3|\Psi_{E_1}\rangle = i\int_{-\infty}^{\infty}\Psi^*_{E_2}(z)\frac{\partial^3\Psi_{E_1}(z)}{\partial z^3}dz + imV_0[\Psi^*_{\Omega,E_2}(w)\Psi_{\Omega,E_1}(w)-\Psi^*_{\Omega,E_2}(-w)\Psi_{\Omega,E_1}(-w)]. \tag{B34}$$

3. Regularization for matrix Schrödinger equations

Finally, we consider quantum wells described by matrix Schrödinger equations

$$-\hat{M}_2\frac{\partial^2\hat{\Psi}(z)}{\partial z^2}-i\hat{M}_1\frac{\partial\hat{\Psi}(z)}{\partial z}+\hat{M}_0\hat{\Psi}(z)+V(z)\hat{I}\hat{\Psi}(z)=E\hat{\Psi}(z), \tag{B35}$$

where $\hat{M}_1$, $\hat{M}_2$ and $\hat{M}_3$ are $n\times n$ matrices, $\hat{I}$ is the $n\times n$ identity and $\hat{\psi}$ is a column of n functions. We assume that M_2 is a diagonal matrix with positive and constant elements $[M_2]_{ii}=1/(2m_i)$. The potential V corresponds to an infinite well as in Eq. (B1). We apply the same regularization procedure for the potential (Fig. 18)

$$V_{\Omega,i}(z)=\begin{cases}0, & \text{if} \quad |z|\leqslant w,\\ \frac{\Omega^2}{2m_i}(z-w)^2, & \text{if} \quad z>w,\\ \frac{\Omega^2}{2m_i}(z+w)^2, & \text{if} \quad z<-w,\end{cases} \tag{B36}$$

Outside the quantum well, the above equation is written using a transformation to the variable $\xi=\sqrt{2\Omega}(z\pm w)$ as

$$-\frac{\partial^2\Psi_{\Omega,i}(\xi)}{\partial\xi^2}-im_i\sqrt{\frac{2}{\Omega}}(\hat{M}_1)_{ij}\frac{\partial\Psi_{\Omega,j}(\xi)}{\partial\xi}+\frac{m_i}{\Omega}(\hat{M}_0)_{ij}\Psi_{\Omega,j}(\xi)+\frac{\xi^2}{4}\Psi_{\Omega,i}(\xi)=\frac{m_iE_\Omega}{\Omega}\Psi_{\Omega,i}(\xi), \tag{B37}$$

where $+$ signs refer to the left side of the well and $-$ to the right side. In the limit of $\Omega\to\infty$, it reads

$$-\frac{\partial^2\Psi_{\Omega,i}(\xi)}{\partial\xi^2}+\frac{\xi^2}{4}\Psi_{\Omega,i}(\xi)=0. \tag{B38}$$

Imposing the requirement that $\hat{\psi}(\pm\infty)=0$, we find the solutions

$$\Psi_{\pm,\Omega i}(\xi)=\alpha_{\pm,i}D_{-\frac{1}{2}}(\pm\xi). \tag{B39}$$

The procedure is identical to the previous case, although the wave functions are now n vectors. The final result reads

$$\left\langle\hat{\Psi}_{E_2}\left|\hat{P}k_z^3\right|\hat{\Psi}_{E_1}\right\rangle = i\int_{-w}^{w}\hat{\Psi}^*_{E_2}(z)\hat{P}\frac{\partial^3\Psi_{E_1}(z)}{\partial z^3}dz+\frac{i}{2}\hat{\Psi}'^*_{E_2}(w)\hat{P}\hat{\Psi}'_{E_1}(w)-\frac{i}{2}\hat{\Psi}'^*_{E_2}(-w)\hat{P}\hat{\Psi}'_{E_1}(-w), \tag{B40}$$

where $\hat{P}$ is a matrix with constant elements.

APPENDIX C: MATRIX ELEMENTS OF THE DRESSELHAUS SPIN-ORBIT INTERACTION

The following matrix elements of terms contributing to the Dresselhaus interactions given by Eq. (56) have nonzero values:

$$\langle\Psi^{(n+4,-p)}|\sum_i J_i\hat{\kappa}_i|\Psi^{(n,p)}\rangle = -\sqrt{\frac{3(n+1)(n+2)(n+3)}{8}}I^{4,0}_{1,0}(n,p)-\sqrt{\frac{n(n+1)(n+2)}{2}}I^{4,0}_{2,1}(n,p)$$
$$-\sqrt{\frac{3(n-1)n(n+1)}{8}}I^{4,0}_{3,2}(n,p), \tag{C1}$$

$$\langle\Psi^{(n+2,-p)}|\sum_i J_i\hat{\kappa}_i|\Psi^{(n,p)}\rangle = -\frac{3i}{2}\sqrt{(n+1)(n+2)}I^{2,1}_{0,0}(n,p) - \frac{i}{2}\sqrt{n(n+1)}I^{2,1}_{1,1}(n,p) + \frac{i}{2}\sqrt{(n-1)n}I^{2,1}_{2,2}(n,p) + \frac{3i}{2}\sqrt{(n-1)(n-2)}I^{2,1}_{3,3}(n,p), \tag{C2}$$

$$\begin{aligned}\langle\Psi^{(n,-p)}|\sum_i J_i\hat{\kappa}_i|\Psi^{(n,p)}\rangle &= \sqrt{\frac{3n^3}{8}}\left[I^{0,0}_{1,0}(n,p)+I^{0,0}_{0,1}(n,p)\right] + \sqrt{\frac{(n-1)^3}{2}}\left[I^{0,0}_{2,1}(n,p)+I^{0,0}_{1,2}(n,p)\right]\\ &+\sqrt{\frac{3(n-2)^3}{8}}\left[I^{0,0}_{2,3}(n,p)+I^{0,0}_{3,2}(n,p)\right] + \sqrt{\frac{3n}{2}}\left[I^{0,2}_{0,1}(n,p)+I^{0,2}_{1,0}(n,p)\right]\\ &+\sqrt{2(n-1)}\left[I^{0,2}_{1,2}(n,p)+I^{0,2}_{2,1}(n,p)\right] + \sqrt{\frac{3(n-2)}{2}}\left[I^{0,2}_{2,3}(n,p)+I^{0,2}_{3,2}(n,p)\right],\end{aligned} \tag{C3}$$

$$\begin{aligned}\langle\Psi^{(n+4,-p)}|\sum_i J_i^3\hat{\kappa}_i|\Psi^{(n,p)}\rangle &= -\frac{7}{8}\sqrt{\frac{3(n+1)(n+2)(n+3)}{2}}I^{4,0}_{1,0}(n,p) - \frac{5}{2}\sqrt{\frac{n(n+1)(n+2)}{2}}I^{4,0}_{2,1}(n,p)\\ &-\frac{7}{8}\sqrt{\frac{3(n-1)n(n+1)}{2}}I^{4,0}_{3,2}(n,p) + \frac{3}{4}\sqrt{\frac{(n+1)^3}{2}}I^{4,0}_{3,0}(n,p)\\ &+\frac{3}{4}\sqrt{2(n+1)}I^{4,2}_{3,0}(n,p),\end{aligned} \tag{C4}$$

$$\langle\Psi^{(n+2,-p)}|\sum_i J_i^3\hat{\kappa}_i|\Psi^{(n,p)}\rangle = -\frac{27i}{8}\sqrt{(n+1)(n+2)}I^{2,1}_{0,0}(n,p) - \frac{i}{8}\sqrt{n(n+1)}I^{2,1}_{1,1}(n,p) + \frac{i}{8}\sqrt{(n-1)n}I^{2,1}_{2,2}(n,p) + \frac{27i}{8}\sqrt{(n-1)(n-2)}I^{2,1}_{3,3}(n,p), \tag{C5}$$

$$\begin{aligned}\langle\Psi^{(n,-p)}|\sum_i J_i^3\hat{\kappa}_i|\Psi^{(n,p)}\rangle &= \frac{7}{8}\sqrt{\frac{3n^3}{2}}\left[I^{0,0}_{1,0}(n,p)+I^{0,0}_{0,1}(n,p)\right] + \frac{5}{2}\sqrt{\frac{(n-1)^3}{2}}\left[I^{0,0}_{2,1}(n,p)+I^{0,0}_{1,2}(n,p)\right]\\ &+\frac{7}{8}\sqrt{\frac{3(n-2)^3}{2}}\left[I^{0,0}_{2,3}(n,p)+I^{0,0}_{3,2}(n,p)\right] + \frac{7}{8}\sqrt{6n}\left[I^{0,2}_{0,1}(n,p)+I^{0,2}_{1,0}(n,p)\right]\\ &+\frac{5}{2}\sqrt{2n-2}\left[I^{0,2}_{1,2}(n,p)+I^{0,2}_{2,1}(n,p)\right] + \frac{7}{8}\sqrt{6n-12}\left[I^{0,2}_{2,3}(n,p)+I^{0,2}_{3,2}(n,p)\right]\\ &-\frac{3}{4}\sqrt{\frac{(n-2)(n-1)n}{2}}\left[I^{0,0}_{0,3}(n,p)+I^{0,0}_{3,0}(n,p)\right],\end{aligned} \tag{C6}$$

$$\langle\Psi^{(n+6,-p)}|\sum_i V_i\hat{\iota}_i|\Psi^{(n,p)}\rangle = \frac{3}{4}\sqrt{\frac{(n+3)(n+2)(n+1)}{2}}I^{6,0}_{3,0}(n,p), \tag{C7}$$

$$\begin{aligned}\langle\Psi^{(n+2,-p)}|\sum_i V_i\hat{\iota}_i|\Psi^{(n,p)}\rangle &= \frac{1}{4}\sqrt{\frac{3(n+2)(n+1)n}{2}}I^{2,0}_{0,1}(n,p) - \frac{3}{4}\sqrt{\frac{(n+1)n(n-1)}{2}}I^{2,0}_{1,2}(n,p)\\ &+\frac{1}{4}\sqrt{\frac{3n(n-1)(n-2)}{2}}I^{2,0}_{2,3}(n,p) + \frac{1}{4}\sqrt{\frac{3(n+1)^3}{2}}I^{2,0}_{1,0}(n,p)\\ &-\frac{3}{4}\sqrt{\frac{n^3}{2}}I^{2,0}_{2,1}(n,p) + \frac{1}{4}\sqrt{\frac{3(n-1)^3}{2}}I^{2,0}_{3,2}(n,p) - \frac{3}{4}\sqrt{\frac{n^3}{2}}I^{2,0}_{3,0}(n,p)\\ &+\frac{3}{4}\sqrt{2n}I^{2,2}_{3,0}(n,p) + \frac{\sqrt{6(n+1)}}{4}I^{2,2}_{1,0}(n,p) - \frac{3}{4}\sqrt{2n}I^{2,2}_{2,1}(n,p)\\ &+\frac{\sqrt{6(n-1)}}{4}I^{2,2}_{3,2}(n,p) + \frac{\sqrt{3}i}{2}(2n+1)I^{2,1}_{2,0}(n,p) - \frac{\sqrt{3}i}{2}(2n-1)I^{2,1}_{3,1}(n,p)\end{aligned} \tag{C8}$$

$$\langle\Psi^{(n+6,-p)}|\sum_i V_i\hat{k}_i^3|\Psi^{(n,p)}\rangle = -\frac{3}{4}\sqrt{\frac{(n+3)(n+2)(n+1)}{2}}I^{6,0}_{3,0}(n,p), \tag{C9}$$

$$\langle\Psi^{(n+2,-p)}|\sum_i V_i\hat{k}_i^3|\Psi^{(n,p)}\rangle = -\frac{1}{4}\sqrt{\frac{3(n+2)(n+1)n}{2}}I_{0,1}^{2,0}(n,p)+\frac{3}{4}\sqrt{\frac{(n+1)n(n-1)}{2}}I_{1,2}^{2,0}(n,p)$$
$$-\frac{1}{4}\sqrt{\frac{3n(n-1)(n-2)}{2}}I_{2,3}^{2,0}(n,p)-\frac{3}{8}\sqrt{6(n+1)^3}I_{1,0}^{2,0}(n,p)+\frac{9}{8}\sqrt{2n^3}I_{2,1}^{2,0}(n,p)$$
$$-\frac{3}{8}\sqrt{6(n-1)^3}I_{3,2}^{2,0}(n,p)-\frac{9}{8}\sqrt{2n^3}I_{3,0}^{2,0}(n,p)+\frac{\sqrt{3}i}{2}I_{2,0}^{2,3}(n,p)-\frac{\sqrt{3}i}{2}I_{3,1}^{2,3}(n,p). \quad \text{(C10)}$$

Here, the components of the operator $\hat{\iota}$ are given by

$$\hat{\iota}_i = \{\hat{k}_i, (\hat{k}^2{}_{i-1}+\hat{k}_{i-2}^2)\}, \quad \text{(C11)}$$

where cyclic permutation of indices is implied. The superposition integral $I_{i,j}^{\Delta,m}(n,p)$ is defined as

$$I_{i,j}^{\Delta,m}(n,p)=\int_{-w}^{w}\left(\zeta_i^{n+\Delta,p'}(z)\right)^*\frac{\partial^m}{\partial z^m}\zeta_j^{n,p}(z)dz+K_{i,j}^{\Delta}(n,p), \quad \text{(C12)}$$

which is nonzero only if $p'=(-1)^{i+j+m}p$. The evaluation of this integral gives

$$I_{i,j}^{\Delta,m}(n,p)=4wi^m\sum_{\alpha,\beta}\left(\lambda_{q_\alpha,i}^{n+\Delta,p'}\right)^*\lambda_{q_\beta,j}^{n,p}q_\beta^m\{\mathrm{sinc}[(q_\beta-q_\alpha^*)w]+(-1)^{j+m}p\,\mathrm{sinc}[(q_\beta+q_\alpha^*)w]\}. \quad \text{(C13)}$$

The quantity $K_{i,j}^{\Delta}(n,p)$ is the correction due to the regularization procedure described in Appendix B, for $m=3$, which is given by

$$K_{i,j}^{\Delta}(n,p)=-2\sum_{\alpha,\beta}q_\alpha^*q_\beta\left(\lambda_{q_\alpha,i}^{n+\Delta,p'}\right)^*\lambda_{q_\beta,i}^{n,p}\{\sin[(q_\beta-q_\alpha^*)w]+p(-1)^{j+1}\sin[(q_\beta+q_\alpha^*)w]\}. \quad \text{(C14)}$$

APPENDIX D: MATRIX ELEMENTS OF NONAXIAL PERTURBATION

The following matrix elements of the nonaxial term described by Eq. (59) have nonzero values:

$$\langle\Psi^{(n+4,-p)}|J_-^2(a^\dagger)^2|\Psi^{(n,p)}\rangle=2\sqrt{3}\left[\sqrt{(n+2)(n+2)}I_{3,0}^{4,0}(n,p)+\sqrt{n(n+1)}I_{4,1}^{4,0}(n,p)\right]. \quad \text{(D1)}$$

[1] L. Fu and C. L. Kane, Phys. Rev. Lett. **100**, 096407 (2008).
[2] R. M. Lutchyn, J. D. Sau, and S. D. Sarma, Phys. Rev. Lett. **105**, 077001 (2010).
[3] Y.-J. Lin, K. Jimenis-Garcia, and I. Spielman, Nature (London) **471**, 84 (2011).
[4] C. L. Kane and E. J. Mele, Phys. Rev. Lett. **95**, 146802 (2005).
[5] M. Konig, S. Wiedmann, C. Brune, A. Roth, H. Buhmann, L. W. Molenkamp, X. Qi, and S. Zhang, Science **318**, 766 (2007).
[6] J. Kikkawa, I. Smorchkova, N. Samarth, and D. Awschalom, Science **277**, 1284 (1997).
[7] A. Imamoğlu, D. D. Awschalom, G. Burkard, D. P. DiVincenzo, D. Loss, M. Sherwin, and A. Small, Phys. Rev. Lett. **83**, 4204 (1999).
[8] J. B. Miller, D. M. Zumbühl, C. M. Marcus, Y. B. Lyanda-Geller, D. Goldhaber-Gordon, K. Campman, and A. C. Gossard, Phys. Rev. Lett. **90**, 076807 (2003).
[9] H. L. Stormer, Z. Schlesinger, A. Chang, D. C. Tsui, A. C. Gossard, and W. Wiegmann, Phys. Rev. Lett. **51**, 126 (1983).
[10] J. P. Eisenstein, H. L. Störmer, V. Narayanamurti, A. C. Gossard, and W. Wiegmann, Phys. Rev. Lett. **53**, 2579 (1984).
[11] B. Habib, E. Tutuc, S. Melinte, M. Shayegan, D. Wassermann, S. A. Lyon, and R. Winkler, Phys. Rev. B **69**, 113311 (2004).
[12] L. P. Rokhinson, V. Larkina, Y. B. Lyanda-Geller, L. N. Pfeiffer, and K. W. West, Phys. Rev. Lett **93**, 146601 (2004).
[13] E.Tutuc, E. P. de Poortere, S. J. Papadakis, and M. Shayegan, Phys. Rev. Lett. **86**, 2858 (2001).
[14] S. Pedersen, C. B. Sørensen, A. Kristensen, P. E. Lindelof, L. E. Golub, and N. S. Averkiev, Phys. Rev. B **60**, 4880 (1999).
[15] L. P. Rokhinson, Y. Lyanda-Geller, Z. Ge, S. Shen, X. Liu, M. Dobrowolska, and J. K. Furdyna, Phys. Rev. B **76**, 161201(R) (2007).
[16] G. Bastard, J. Brum, and R. Ferreira, *Electronic States in Semiconductor Heterostructures*, edited by H. Ehrenreich and D. Turnbull, Solid State Physics Vol. 44 (Academic Press, New York, 1991).
[17] D. P. Arovas and Y. Lyanda-Geller, Phys. Rev. B **57**, 12302 (1998).
[18] D. V. Bulaev and D. Loss, Phys. Rev. Lett. **98**, 097202 (2007).
[19] B. A. Bernevig and S.-C. Zhang, Phys. Rev. Lett. **95**, 016801 (2005).
[20] J. Schliemann and D. Loss, Phys. Rev. B **71**, 085308 (2005).
[21] B. A. Glavin and K. W. Kim, Phys. Rev. B **71**, 035321 (2005).
[22] Y. B. Lyanda-Geller, T. L. Reinecke, and M. Bayer, Phys. Rev. B **69**, 161308 (2004).
[23] D. Csontos, P. Brusheim, U. Zuelicke, and H. Q. Xu, Phys. Rev. B **79**, 155323 (2009).
[24] M. Zarea and S. E. Ulloa, Phys. Rev. B **73**, 165306 (2006).

[25] C.-X. Liu, B. Zhou, S.-Q. Shen, and B.-f. Zhu, Phys. Rev. B **77**, 125345 (2008).

[26] S. Chesi, G. F. Giuliani, L. P. Rokhinson, L. N. Pfeiffer, and K. W. West, Phys. Rev. Lett. **106**, 236601 (2011).

[27] D. A. Broido and L. J. Sham, Phys. Rev. B **31**, 888 (1985).

[28] S.-R. Eric Yang, D. A. Broido, and L. J. Sham, Phys. Rev. B **32**, 6630 (1985).

[29] U. Ekenberg and M. Altarelli, Phys. Rev. B **32**, 3712 (1985).

[30] Y.-C. Chang and J. N. Schulman, Phys. Rev. B **31**, 2069 (1985).

[31] K. Rachor, T. E. Raab, D. Heitmann, C. Gerl, and W. Wegscheider, Phys. Rev. B **79**, 125417 (2009).

[32] R. Winkler, *Spin-Orbit Coupling Effects in Two-Dimensional Electron and Hole Systems*, Springer Tracts in Modern Physics (Springer, Berlin, 2003).

[33] J. M. Luttinger, Phys. Rev. **102**, 1030 (1956).

[34] S. Nedorezov, Sov. Phys. Solid State **12**, 1814 (1971) [Fizika Tverdogo Tela **12**, 2269 (1970)].

[35] I. Merkulov, V. Perel', and M. Portnoi, Sov. Phys. JETP **72**, 669 (1991) [Zh. Eksp. Teor. Fiz **99**, 1202 (1991)].

[36] M. D'yakonov and A. Khaetskii, Sov. Phys. JETP **55**, 917 (1982) [Zh. Eksp. Teor. Fiz **82**, 1584 (1982)].

[37] Y. Lyanda-Geller, arXiv:1210.7825.

[38] V. M. Apalkov and M. E. Portnoi, Phys. Rev. B **65**, 125310 (2002).

[39] V. N. Golovach and M. E. Portnoi, Phys. Rev. B **74**, 085321 (2006).

[40] G. Giuliani and G. Vignale., *Quantum Theory of the Electron Liquid* (Cambridge University Press, Cambridge, 2005).

[41] R. Winkler, M. Merkler, T. Darnhofer, and U. Rossler, Phys. Rev. B **53**, 10858 (1996).

[42] E. Rashba and E. Sherman, Phys. Lett. A **129**, 175 (1988).

[43] G. L. Bir, E. I. Butikov, and G. E. Pikus, Sov. Phys. Solid State **9**, 835 (1967) [Fizika Tverdogo Tela **9**, 1068 (1967)].

[44] J. Hopfield, J. Phys. Chem. Solids **15**, 97 (1960).

[45] G. Simion and Y. Lyanda-Geller (unpublished).

[46] Y. Liu, S. Hasdemir, D. Kamburov, A. L. Graninger, M. Shayegan, L. N. Pfeiffer, K. W. West, K. W. Baldwin, and R. Winkler, Phys. Rev. B **89**, 165313 (2014).

[47] Y. Liu, A. L. Graninger, S. Hasdemir, M. Shayegan, L. N. Pfeiffer, K. W. West, K. W. Baldwin, and R. Winkler, Phys. Rev. Lett. **112**, 046804 (2014).

[48] S. Glasberg, H. Shtrikman, and I. Bar-Joseph, Phys. Rev. B **63**, 201308 (2001).

[49] H. Zhu, K. Lai, D. Tsui, S. Bayrakci, N. Ong, M. Manfra, L. Pfeiffer, and K. West, Solid State Commun. **141**, 510 (2007).

[50] T. M. Lu, Z. F. Li, D. C. Tsui, M. J. Manfra, L. N. Pfeiffer, and K. W. West, Appl. Phys. Lett. **92**, 012109 (2008).

[51] M. N. Khannanov, I. V. Kukushkin, V. E. Bisti, Y. A. Nefyodov, and S. I. Gubarev, JETP **107**, 587 (2008) [Zh. Eksp. Teor. Fiz. **134**, 687 (2008)].

[52] G. Dresselhaus, A. F. Kip, and C. Kittel, Phys. Rev. **98**, 368 (1955).

[53] E. Rashba, Sov. Phys. Solid State **2**, 1109 (1960).

[54] E. L. Ivchenko and G. E. Pikus, *Superlattices and Other Heterostructures : Symmetry and Optical Phenomena*, 2nd ed. (Springer, Berlin, 1997).

[55] T. Darnhofer, U. Rössler, and D. A. Broido, Phys. Rev. B **52**, R14376 (1995).

[56] W. Kohn, Phys. Rev. **123**, 1242 (1961).

[57] V. Kirpichev, I. Kukushkin, V. E. Bisti, K. von Klitzing, and K. Elbert, JETP Lett. **64**, 814 (1996) [Pis'ma Zh. Eksp. Teor. Fiz. **64**, 766 (1996)].

[58] F. Nichele, A. N. Pal, R. Winkler, C. Gerl, W. Wegscheider, T. Ihn, and K. Ensslin, Phys. Rev. B **89**, 081306 (2014).

[59] B. P. Zakharchenya, D. N. Mirlin, V. I. Perel', and I. I. Reshina, Soviet Physics Uspekhi **25**, 143 (1982).

[60] B. Zakharchenya, P. Kop'ev, D. Mirlin, D. Polakov, I. Reshina, V. Sapega, and A. Sirenko, Solid State Commun. **69**, 203 (1989).

[61] V. Timofeev, M. Bayer, A. Forchel, and M. Potemski, JETP Lett. **64**, 57 (1996).

[62] O. Carmel, H. Shtrikman, and I. Bar-Joseph, Phys. Rev. B **48**, 1955 (1993).

[63] H. Wang, M. Jiang, R. Merlin, and D. G. Steel, Phys. Rev. Lett. **69**, 804 (1992).

[64] V. F. Sapega, M. Cardona, K. Ploog, E. L. Ivchenko, and D. N. Mirlin, Phys. Rev. B **45**, 4320 (1992).

[65] A. Arora, A. Mandal, S. Chakrabarti, and S. Ghosh, J. Appl. Phys. **113**, 213505 (2013).

[66] Y. H. Chen, X. L. Ye, B. Xu, Z. G. Wang, and Z. Yang, Appl. Phys. Lett. **89**, 051903 (2006).

[67] S. P. Koduvayur, L. P. Rokhinson, D. C. Tsui, L. N. Pfeiffer, and K. W. West, Phys. Rev. Lett. **100**, 126401 (2008).

[68] A. Srinivasan, L. A. Yeoh, O. Klochan, T. P. Martin, J. C. H. Chen, A. P. Micolich, A. R. Hamilton, D. Reuter, and A. D. Wieck, Nano Lett. **13**, 148 (2013).

[69] R. Danneau, O. Klochan, W. R. Clarke, L. H. Ho, A. P. Micolich, M. Y. Simmons, A. R. Hamilton, M. Pepper, D. A. Ritchie, and U. Zülicke, Phys. Rev. Lett. **97**, 026403 (2006).

[70] R. Winkler, S. J. Papadakis, E. P. De Poortere, and M. Shayegan, Phys. Rev. Lett. **85**, 4574 (2000).

[71] T. Ando and Y. Uemura, J. Phys. Soc. Jpn. **37**, 1044 (1974).

[72] B. M. Gorbovitski'i and V. I. Perel', Sov. Phys. JETP **58**, 1054 (1983) [Zh. Eksp. Teor. Fiz **85**, 1812 (1983)].

[73] J. Keller, Ann. Phys. **4**, 180 (1958).

[74] J. Keller and S. Rubinov, Ann. Phys. **9**, 24 (1960).

[75] S. I. Dorozhkin, Phys. Rev. B **41**, 3235 (1990).

[76] M. V. Durnev, M. M. Glazov, and E. L. Ivchenko, Physica E **44**, 797 (2012).

[77] G. Dresselhaus, Phys. Rev. **100**, 580 (1955).

[78] K. V. Kavokin and M. E. Portnoi, Semiconductors **42**, 989 (2008).

[79] G. Pikus, V. Marushchak, and A. Titkov, Sov. Phys. Semicond. **22**, 115 (1988) [Fiz. Tekh. Poluprovodn **22**, 185 (1988)].

[80] D. V. Bulaev and D. Loss, Phys. Rev. Lett. **95**, 076805 (2005).

[81] M. V. Durnev, M. M. Glazov, and E. L. Ivchenko, Phys. Rev. B **89**, 075430 (2014).

[82] T. Ando, A. B. Fowler, and F. Stern, Rev. Mod. Phys. **54**, 437 (1982).

[83] http://www.functions.wolfram.com/HypergeometricFunctions/ParabolicCylinderD/